ABSTRACT

LOWE, LISA BIZZELL. Synthesis and Characterization of a Dye Sensitizing Molecule for Photoelectrochemical DNA Hybridization Detection. (Under the direction of Daniel L. Feldheim.)

A procedure for detection of DNA hybridization is described for the purpose of application in DNA microarray technology. The approach is based on the attachment of a dye-sensitizing molecule to the target oligonucleotide and detection of hybridization of this target to its complementary, surface-attached probe by photoelectrochemistry. A thiolated ruthenium (II) tris(2,2'-bipyridine) dye was synthesized and characterized. The target oligonucleotide was attached to a 10nm gold colloid before hybridization to the probe oligonucleotide, which was immobilized on a polycrystalline gold substrate. Upon hybridization the gold substrate was exposed to the thiolated $[Ru(bpy)_3]^{2+}$, allowing attachment of the molecule to the gold nanoparticles. The photoelectrochemical response was dependent upon applied potential and target concentration. Attachment of the probe oligonucleotide to the gold substrate was investigated, and the electrolyte solution was tested for optimal performance.

SYNTHESIS AND CHARACTERIZATION OF A DYE SENSITIZING MOLECULE FOR PHOTOELECTROCHEMICAL DNA HYBRIDIZATION DETECTION

by

LISA BIZZELL LOWE

A thesis submitted to the Graduate Faculty of
North Carolina State University
in partial fulfillment of the requirements
for the Degree of
Masters of Science

DEPARTMENT OF CHEMISTRY

Raleigh, North Carolina

July 2002

APPROVED BY:

Dr. Stefan Franzen

Dr. Charles Boss

Dr. Daniel L. Feldheim
Chair of Advisory Committee

DEDICATION

This work is dedicated to my mother, Linda Sanders Bizzell, who was the source of much encouragement throughout my high school and college years. This work is also dedicated to my late father, Melvin Ray Bizzell, whose efforts in agriculture sparked my interest in the science field.

BIOGRAPHY

Lisa Bizzell Lowe was born on June 22, 1975 in Orangeburg, South Carolina. She was raised on a farm outside of Norway, SC along with one brother and three sisters, one her fraternal twin. Lisa attended high school at Heritage Hall Academy where she was the class of 1993 valedictorian and a member of the last graduating class of Heritage Hall before the school merged with Andrew Jackson Academy in Ehrhardt, SC. Lisa graduated from the College of Charleston with honors in May 1997, obtaining a Bachelor of Science in Biology. She then moved to Pensacola, Florida where she worked as a microbiologist at the University of West Florida then a chemist at Severn Trent Laboratories, Inc., both jobs pertaining to environmental analysis. After marrying Sean Ellington Lowe in Charleston, SC in September of 1998, the couple remained in Pensacola, FL until July 1999 when they moved to Clayton, North Carolina. Lisa spent the following three years working on her Masters of Science degree from the Department of Chemistry at North Carolina State University in Raleigh, NC.

ACKNOWLEDGEMENTS

Dr. Daniel L. Feldheim

Dr. Stefan Franzen

Feldheim Group

Dr. Robert C. Tenent

Sofi Bin-Salamon

Franzen Group Members:

Selina J. Anthireya

Scott Brewer

Derek Brown

Simon Lappi

Research Funded by Applied Biosystems, Inc.

Tim Woudenberg

Tim Liu

TABLE OF CONTENTS

LIST OF TABLES

TABLE OF FIGURES

Chapter 1: Introduction and Background

1.1 Introduction

All human cells have a nucleus that contains a person's genetic fingerprint known as DNA. Three billion chemical bases make up human DNA forming an estimated 50,000 – 100,000 genes in what is called the human genome. The Human Genome Project is a hunt to locate and then decipher the DNA sequences of all these genes in order to determine which gene sequences is responsible for the 4,000 known genetic disorders. Though great efforts have been put forth, the sequence of only 60 genetic disorders have been identified to date. Investigations of the human genome also focus on determining genetic mutations that lead to diseases and cancer. Over the last 15 years research interests have focused on obtaining this sequence specific information in a manner that is faster, simpler, and less expensive. Much of the research effort has moved to DNA microarrays, or chips, which incorporate DNA hybridization for analysis. These chips may one day allow the analysis of the entire human genome in a single reaction.

DNA hybridization detection first began in the mid-1970s with methods such as the Southern Blot, created by EM Southern in 1975[1]. This is one of the first methods that utilize various single-stranded DNA sequences, known as "probes," and a radioisotope-tagged compliment to one of the probes called the "target". In the attempt to make this process more rapid and easier to use, efforts focused on immobilizing the probe DNA on a solid support in a 2-D array where the location of each probe is known. The target, which can be labeled by means other than radioisotopes, is then identified according to the location in which it hybridizes.

The development of gene sensors has become increasingly important due to its application in the medical, pharmaceutical, and forensic fields as well as the Human

Genome Project. In the early 1990s advances were made in the technology of enzyme sensors, immunosensors, and microbial biosensors, while few studies were available on biosensors incorporating DNA until 1997[2]. DNA biosensors, which utilize DNA hybridization techniques, offer an advantage over many other biosensors in that DNA is very stable and can be readily synthesized or regenerated for recurring use[2,3]. DNA chips also allow true parallelism, miniaturization, and automation that cannot be achieved with the earlier technologies. Microarray assays allow massive parallel data acquisition and analysis. Parallelism greatly increases the speed of experimental progress and allows meaningful comparisons to be made between the genes represented in the microarray. The miniaturization allows thousands of probes to be chemisorbed to a substrate for analysis. Current strategies attempt to increase specificity and sensitivity of these devices by altering the transducing marker in combination with the analysis method. With the advantage of the electrochemical monitoring of the DNA hybridization at the transducer surface would be the low cost and speed of analysis.

This study set out to develop a DNA hybridization technique that is simple, inexpensive, and selective while improving the sensitivity that has been obtained in other methods. A photoredox active molecule will be synthesized in this study and attached to a target oligonucleotide using the well-studied binding of oliogos and other molecules to gold colloid via a Au-S linkage. DNA hybridization will be detected using photoelectrochemical measurements. Key components will be investigated in order to obtain a high signal-to-noise ratio. Future work will be proposed in order to exponentially increase the signal for development of a DNA chip product.

1.2 Background

1.2.1 DNA Hybridization

Strands of deoxyribonucleic acid, or DNA, are long polymers built out of millions of nucleotides (sometimes called nucleotide bases or simply bases). An individual nucleotide consists of three parts: one of four nitrogen bases, deoxyribose, and a phosphate group. As shown in Figure 1.1, deoxyribose is a 5-carbon sugar. The phosphate group, which is hydrophilic, binds to the sugar through the fifth carbon while the base binds to the first carbon. The four hydrophobic bases are adenine (A), guanine (G), thiamine (T), and cytosine (C). A and G are called purines due to their double-ringed structure, and thiamine (T) and cytosine (C) are called pyrimidines since they are single-ringed bases. The phosphate of one nucleotide binds to the third carbon of the sugar through the hydroxyl group, forming a phosphodiester bond. This polymer strand, or single-stranded DNA (ssDNA), is terminated with a phosphate group on the "3'-end" and a hydroxyl group on the "5'-end" (Figure 1.2).

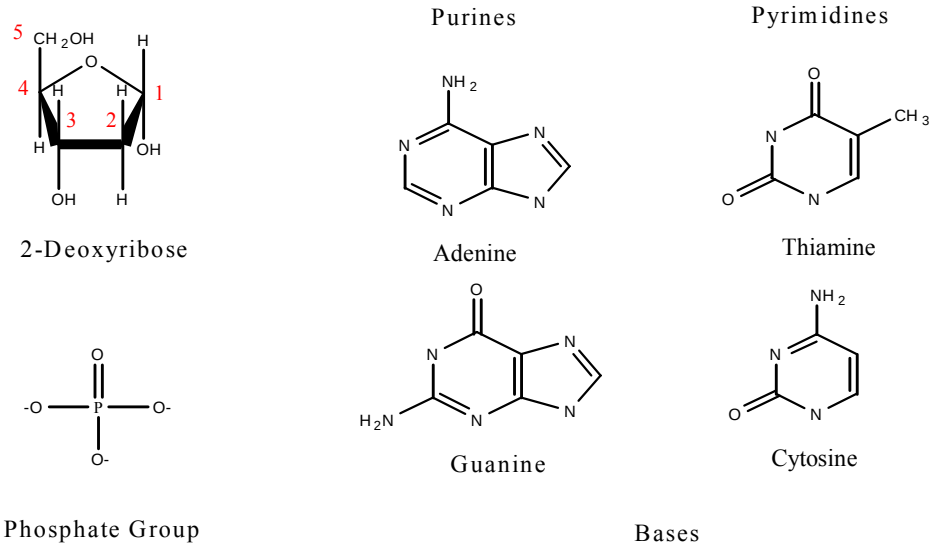

Figure 1.1 DNA Components.

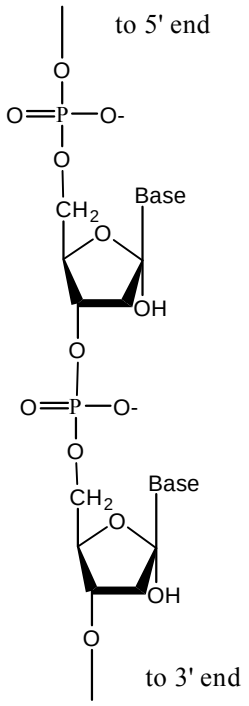

Figure 1.2 Phospho-diester Bond of ssDNA.

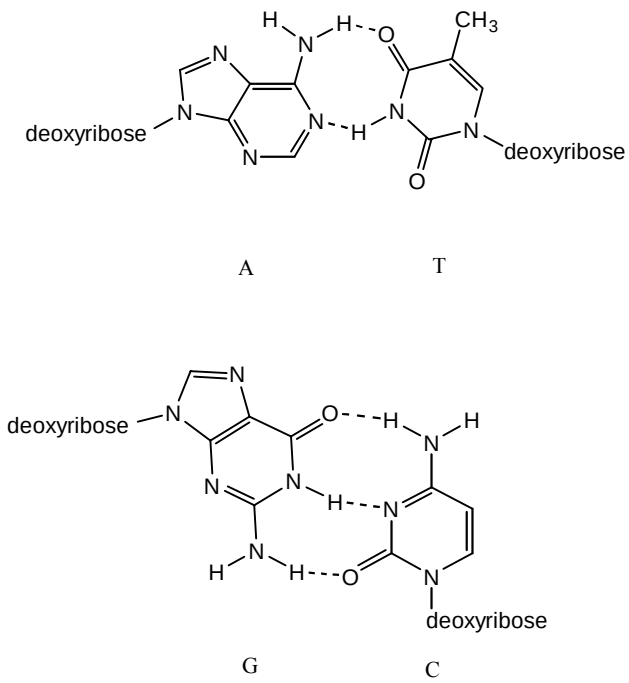

Figure 1.3 Watson-Crick Interactions.

Hybridization is the process of binding two single strands of DNA that contain complementary bases through hydrogen bonding. Figure 1.3 demonstrates how adenine binds to thiamine and guanine binds to cytosine through weak hydrogen bonds, or Watson-Crick interactions, to form a base pair. As this hydrogen bonding occurs, the hydrophobic bases turn to the inside and the phosphates orient themselves to the outside, producing the DNA's familiar double helix shape (Figure 1.4[4]). This binding is a function of temperature, salt concentration (which neutralizes the negative charge on the phosphate

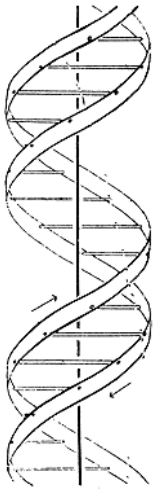

Figure 1.4 DNA Double Helix.

groups), DNA concentration, and base composition. Hybridization is typically performed at a temperature about 25ºC below the melting temperature (the temperature at which half of the DNA strand is separated) for 6 to 18 hours in a 1.0 M salt solution buffered to a pH of 7. After hybridization, double-stranded DNA (dsDNA) may be separated again using a process called melting, where the DNA sample is heated and monitored using UV-Visible Spectroscopy, plotting the absorbance at 260nm versus temperature (Figure 1.5). A-T with its two hydrogen bonds melts at a lower temperature than G-C, and G-C has to be at a lower temperature than A-T to hybridize since it has 3 hydrogen bonds.

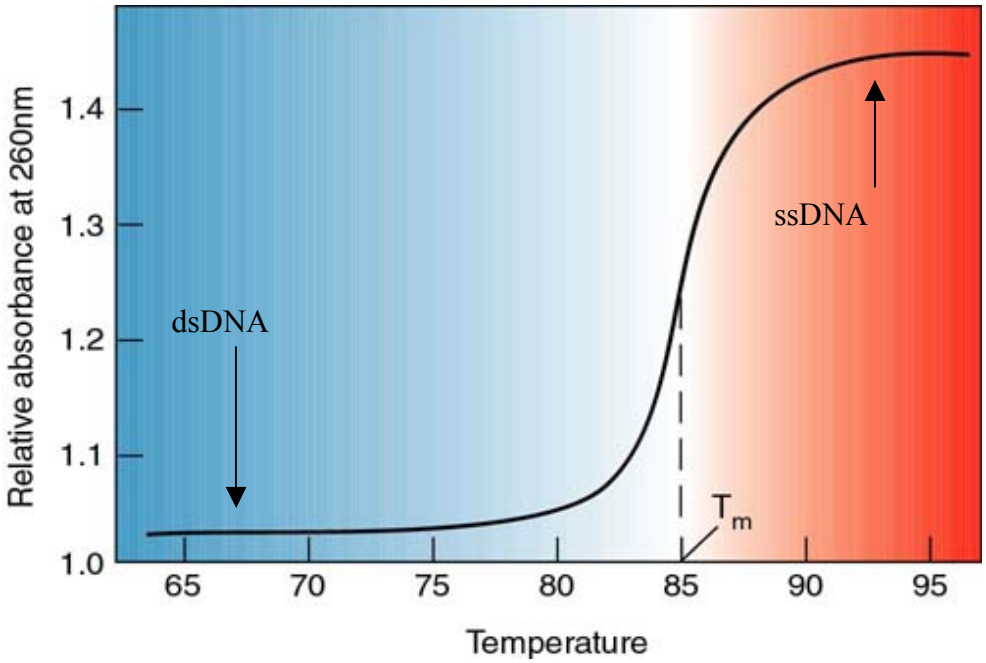

Figure 1.5 DNA Melting Curve.

1.2.2 DNA Microarrays

A DNA microarray, or chip, is a 2-D array of ssDNA "probes" that are immobilized on a solid, non-porous support with the DNA at each location having a known sequence. The number of the DNA samples on the microarray, commonly an area $1cm^2$ in size on a glass microscope slide, can be from a few to a few thousand. The chip is then exposed to an unknown sequence of DNA called the target that may be complementary to one of the known sequences on the chip. After exposure to hybridization conditions, the location of the hybridized target is detected directly or is tagged with some type of marker for indirect detection.

Typically the terms microarray and chip are used interchangeably in the literature; however, there is a historical difference. The method "traditionally" called DNA microarray was developed at Stanford University. In this method, ssDNA (500 – 5,000 bases long) is immobilized to a solid surface and exposed to the targets either separately or in a mixture. The second type of array, the DNA chip which was developed at Affymetrix, Inc who owns the *GeneChip*® trademark, consists of oligonucleotides that are 20-80 bases long that are synthesized either on the chip or synthesized by conventional means and immobilized on the solid support. The array is exposed to the labeled target and analyzed[5]. DNA chip, DNA microarray, oligomer chip, oligomer array, and gene chip are now considered to be the same thing. Most current studies use probes that are short, synthetic strands of DNA, commonly referred to as oligonucleotides or oligomers, in the range of 20-40 base pairs[2]. The production of DNA chips has been accomplished on glass through microspotting, ink-jetting, or photolithography[6,7], which

are outlined in Table 1.1[8]. Derivatives of these techniques can be used for other substrates such as gold.

Table 1.1 Microarray Fabrication Technologies for Glass Slides

Criterion	**Photolithography**	**Piezoelectric**	**Microspotting**
Combinatorial synthesis	Yes	Yes	No
Ink-jetting	No	Yes	No
Surface printing	No	No	Yes
Masks needed	Yes	No	No
Sample tracking	No	No	Yes
Density (cm^{-2})	244 000	10 000	6500
Length restriction	~τν 52	None	None
Array elements	Oligos only	Oligos and cDNAs	Oligos and cDNAs
Prototyping cost	High	Moderate	Low
Applications	Gene expression, Mutation detection	Gene expression, Mutation detection	Gene expression, Mutation detection

1.2.2 Detecting Target Hybridization

1.2.3.1 Electrochemical Detection

Hybridization can be detected either directly, through detection of the DNA itself, or indirectly by labeling the target with a transducing marker or detecting molecules that interact with DNA. Most direct methods depend on electrochemical properties of DNA. One common method used for direct detection focuses on the oxidation and reduction of the DNA bases. DNA contains three electroactive groups, which are adenine, guanine, and cytosine. Adenine has been shown to electrochemically oxidize on graphite electrodes and guanine on both graphite and mercury electrodes while adenine and cytosine can be electrochemically reduced on a mercury electrode. Deoxyribose and the phosphate group are not reducible by electrochemical methods[9]. The oxidation and reduction sites of these molecules are shown in Figure 1.6[10]. Adenine and cytosine are electrochemically reduced in an area of the molecule that contains hydrogen bonds. The

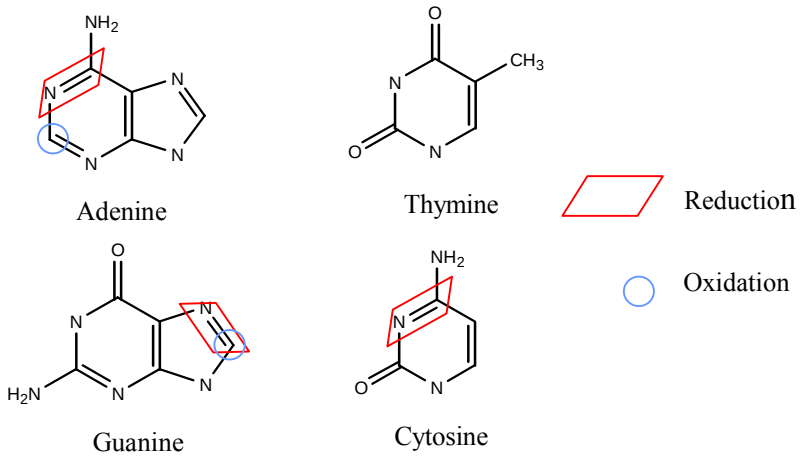

Figure 1.6 Oxidation and Reduction Sites of the DNA Bases.

reduction of these two molecules includes protonation, which takes place at neutral pH. The reduction pathways are demonstrated in Figure 1.7. Oxidation of adenine and

guanine, on the other hand, do not involve hydrogen bonds. The suggested pathways for this oxidation are in Figure 1.8[9].

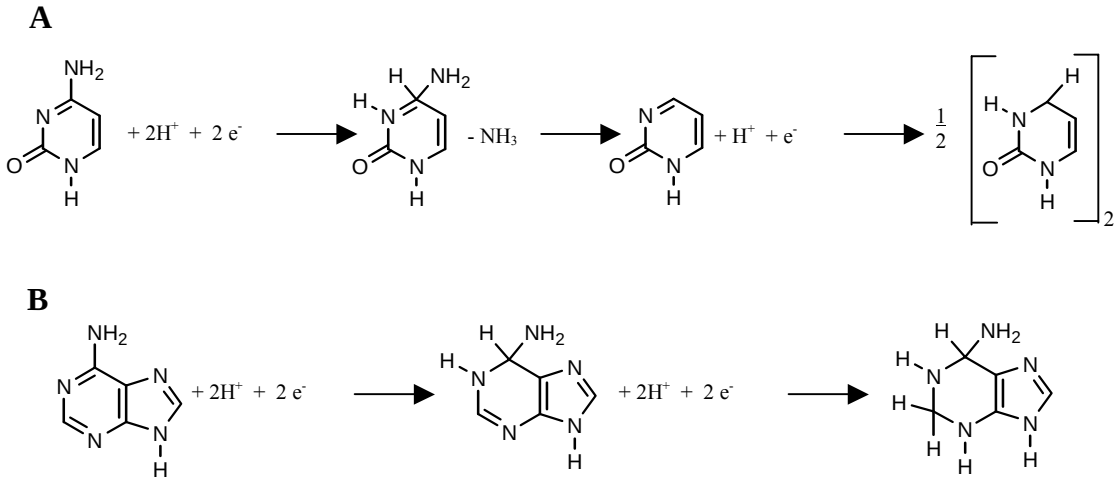

Figure 1.7 Pathways for Electrochemical Reduction of Cytosine (A) and Adenine (B) at HDME.

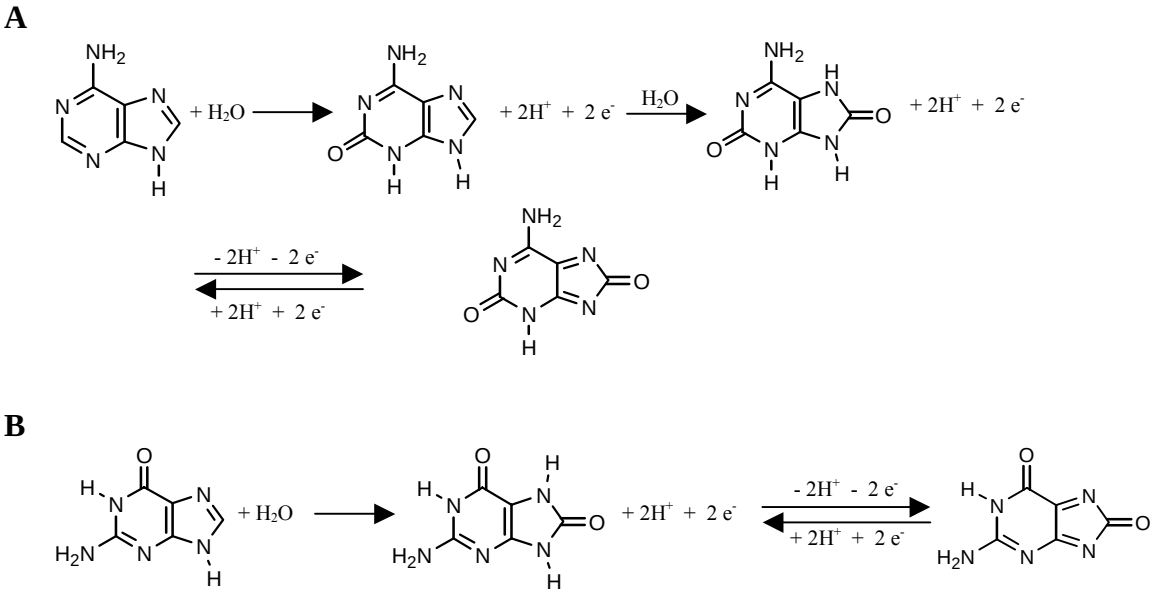

Figure 1.8 Pathways for Electrochemical Oxidation of Adenine (A) and Guanine (B) at a Graphite Electrode.

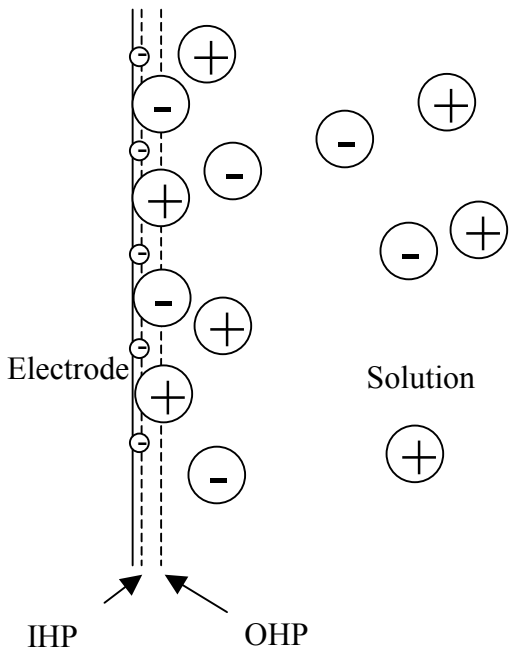

Figure 1.9 Helmholtz Model. Proposed model of the double-layer region under conditions where anions are specifically adsorbed. IHP is the inner Helmholtz Plane and OHP is the outer.

Another electrochemical method used for hybridization detection is Electrochemical Impedance Spectroscopy (EIS). In an electrochemical cell, solvent molecules adsorb to the working electrodes surface which is demonstrated in Figure 1.9. The equivalent circuit of this system is in Figure 1.10. The values of the solution resistance, R_{Ω}, and capacitance due to the double layer, C_d, are measurable using EIS. When DNA is immobilized on an electrode, an additional capacitive layer is formed, C_{ads}, as well as resistance due to charge transfer through the molecule, R_{ct} (Figure 1.11). These values change depending on the presence of double-stranded or single-stranded DNA.

Yassar et al.[11] performed direct electrochemical assay of double-stranded DNA using the first method described above, but this method revealed low sensitivity and selectivity. Thorp et al.[12,13] on the other hand have been able to detect 10^{-12}M DNA hybridized to a surface by increasing sensitivity using electrocatalytic oxidation of guanine with $[Ru(bpy)_3]^{2+}$. While this improvement in sensitivity is remarkable it is not applicable to a DNA microarray since it involves detection of guanine, which can be

found in all DNA. Willner et al.[14] reported using EIS to demonstrate selectivity as well as sensitivity. Binding avidin to a biotin-tagged target increased sensitivity even more.

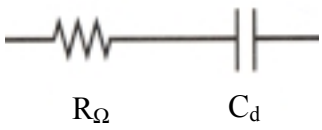

Figure 1.10 Equivalent Circuit of and Electrochemical Cell.

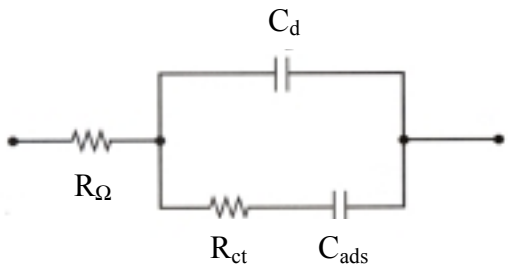

Figure 1.11 Equivalent Circuit of DNA Self-Assembled Monolayer.

Indirect DNA hybridization detection using electrochemistry typically involves attaching a redox active molecule to the target and detecting by cyclic voltammetry. These electroactive hybridization indicators were among the first labels used for binding recognition[15,16] and are still being investigated for possible use in DNA chips. The original redox active sensors dating back to the early 1990s lacked sensitivity and selectivity. More recent research shows an improvement in selectivity, completely distinguishing between matched and mismatched sequences[17,18]. Meade et al.[19] used ferrocene as a redox marker and R.M. Umek patented the technique using ferrocene and ruthenium based molecules[20]. Sensitivity has also improved with a detection limit of 10 zmol[21].

1.2.3.2 Optical Detection Methods

Radioisotopes were among the first tags studied, however, due to the hazards of handling this material and disposing of it, research quickly moved to safer optical methods such as fluorescence, Surface Plasmon Resonance (SPR), and colloid labeling. Optical labels for targets have shown promising results over the past few years as an indirect means of detection.

Fluorescence is probably one of the most thoroughly studied detection methods with products available from many companies such as Affymetrix, Inc., Gene Logic, and Xenometrix, Inc., just to name a few. With this method multiple targets may be used by tagging with various fluorescent dyes (Figure 1.12). Fluorescence analysis is typically performed in one of two ways. In the first method, ssDNA (500 – 5,000 bases long) is immobilized on a solid surface and exposed to the targets either separately or in a mixture. This method, developed at Stanford University, is "traditionally" called DNA microarray. The second method uses oligonucleotides that are 20-80 bases long that are synthesized either on the chip or by conventional means and immobilized on the solid support. The array is exposed to the labeled target and analyzed. This method was developed at Affymetrix, Inc., which owns the *GeneChip*® trademark, and has "historically" been titled DNA chips[5]. Analysis is usually performed using scanning confocal fluorescence microscopes or a charge-coupled device, both allowing readout of

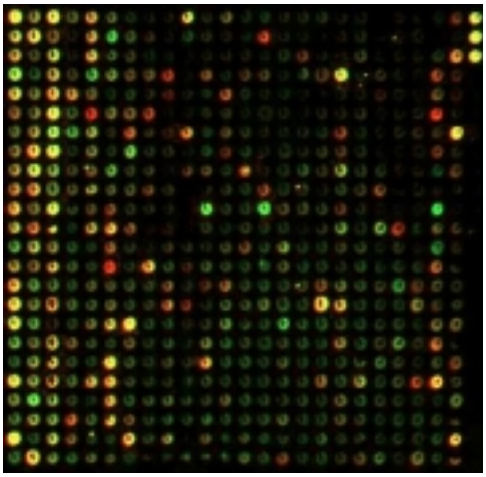

Figure 1.12 Fluorescence-Based Microarray.

the entire array within minutes[22,23]. While this high throughput technology is widely used, it comes with its problems. The preparation of fluorescent-labeled targets is more complex than most target labeling. The process starts with reverse transcription of messenger RNA to obtain the oligonucleotides, which then must be amplified by Polymerase Chain Reaction (PCR) and fluorescent labeled. The sensitivity and selectivity can also be a problem, depending on which of the two methods is used. The first method with longer DNA strands provides many locations for fluorescent labels offering a sensitivity of 1 pM; however, as the number of bases increases, so does the chance of non-specific binding. This method has an increased chance for false positives. The second method uses shorter chains, decreasing the probability of non-specific binding. Sensitivity decreases with this method since short oligonucleotides have only a few locations for fluorescent labels.

Another optical method of detection is Surface Plasmon Resonance. When incident light is totally reflected off of a surface, the electromagnetic field component penetrates tens of nanometers into a medium of low refractive index creating what is known as an evanescent wave. When monochromatic, p-polarized light is reflected off of a thin layer of metal, such as gold, the intensity of the reflected light is reduced at a specific incident angle producing Surface Plasmon Resonance (SPR) due to the resonance energy transfer between evanescent wave and surface plasmons. The material adsorbed onto the metal film influences the resonant conditions, causing an observable decrease in reflected light. The SPR signal, expressed in resonance units, is a measure of mass concentration on the surface of the substrate. An instrumental setup is demonstrated in Figure 1.13. SPR can be used as a direct detection method for DNA

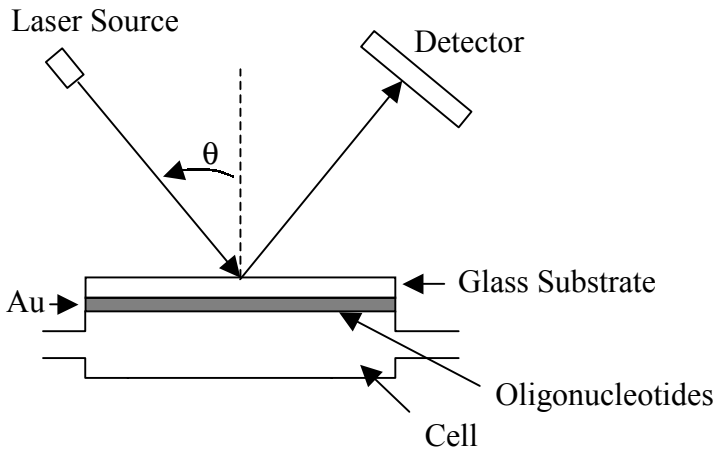

Figure 1.13 SPR Setup.

hybridization, differentiating between single- and double-stranded DNA on a gold surface[24,25]. The sensitivity of these measurements allowed for a detection of 10^{11} molecules/cm^2. Attaching biotin[26] or gold colloid[27,28] to the target oligo, reaching detection limits comparable to that of fluorescence methods, 10 pM (≤ 8 x 10^8 molecules/cm^2), has increased this sensitivity. The study using a biotin-labeled target demonstrated amplification in signal by exposing the hybridized DNA to streptavidin, which binds to biotin. This research also demonstrated that the presence of DNA in solution does not interfere with the detection of hybridization at the surface. Atomic Force Microscopy (AFM) or Scanning Tunnelling Microscopy (STM) can be used with the gold colloid technique in order to obtain a surface coverage of the hybridized DNA since one gold colloid represents one DNA binding site.

1.2.3.3 Colloid Labeling

Gold nanoparticles have been used in combination with SPR (as mentioned above) to amplify the signal. Nanoparticles have also been used unaccompanied by other detection methods for optical detection. Fritzsche et al.[29] attached 30nm colloidal gold to

the 20-mer targets before exposing the target to a DNA chip as a proof of concept. Transmission and reflection microscopy were used for detection and AFM for verification. While this technique did result in some non-specific binding, it did prove to be very stable in comparison to fluorescence, which may undergo bleaching over time. Simon et al.[30] demonstrated the same concept using 40nm gold colloid attached to a 24-mer. Detection using AFM also showed a very small amount of non-specific binding that is much lower than that of fluorescence techniques. Mirkin et al.[31,32] used a flatbed scanner for detection in a scheme where gold and silver nanoparticles were used, yielding detection as low as 50 fM. This detection limit is 100 times better than that of fluorescence methods. The selectivity of this method also proved to be 100 times better than that of fluorescence when identical sequences were used.

1.2.3.4 Piezoelectric Detection Methods

Quartz Crystal Microbalance (QCM) techniques allow direct detection of hybridization. This method uses piezoelectric material, quartz crystal, as a microgravimetric detector. When an external voltage is applied, motion occurs between two parallel crystal surfaces. An external circuit maintains crystal relaxation and oscillation at the resonant frequency. When mass is added to the crystal, a change in frequency is observed. DNA hybridization is detected by looking for an increase in mass upon hybridization. Research in the area of piezoelectric detection of DNA hybridization has seen little improvement during recent years[8,33,34,35,36]. Error in selectivity ranges from 30-90%[37] and sensitivity of the mass change is just under 1×10^{-9} g/cm^2 for molecules with a high molecular mass[38].

1.2.4 Electron Transfer through DNA

In a lecture given on March 21, 1941, Nobel laureate Albert Szent-Györgyi speculated that proteins are semiconductors and reasoned that biological molecules could conduct electricity[39,40]. After 1953 when James Watson and Francis Crick discovered the double helix structure of DNA[41], D.D Eley and D.I. Spivey also suggested that DNA could serve as an electronic conductor[42]. Since Barton et al.[43] first reported their discovery that long distance photoinduced electron transfer (more than 40 angstroms) may be mediated by the DNA helix, whether the pi-stack DNA system functions as a molecular wire or an insulator, has been the subject of much interest and dispute. As mentioned in section 1.2.1, the hydrophobic bases turn to the inside of the DNA double helix. The bases stacked along the long axis of the DNA allow some of the electron orbitals belonging to the bases to overlap, creating π-stacking interactions that may facilitate electron transport through DNA. These ideas have resurfaced in the last seven years due to interests in understanding DNA damage associated with many diseases and the potential for use of DNA in molecular electronics.

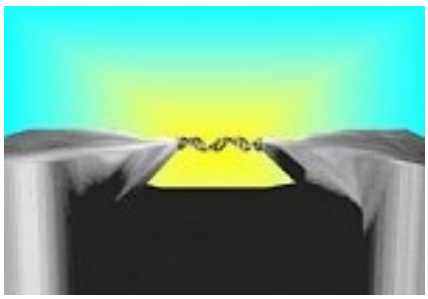

Figure 1.14 Model of DNA molecule extended between two metal contacts.

Over the past 7 years research pertaining to the electroactivity of DNA has given conflicting results. While some say that DNA acts as a molecular "wire,"[44,45,46,47] others disagree, claiming that DNA acts as an insulator[39,48,49,50,51]. In search of an answer, many techniques have been used. These include pulse-radiolysis time-resolved microwave conductivity,[52] fluorescent quenching[53,54], femtosecond transient absorption

measurements[55], and direct measurements of electrical current as a function of the potential applied across a DNA molecule attached to metal contacts (illustrated in Figure 1.14),[49,45,56,57] The major factor of conflicting results in these studies is the sequence of the base pairs along the molecule. Other factors may also affect the charge transport such as temperature, concentration, and solvent. While many of these studies focused on charge transfer over long distances, little was known about transfer of transfer of charge over a short distance. The most important research to date is on short DNA chains, which focuses on charge transport through DNA due to electron tunnelling and hopping[49,58,59,60].

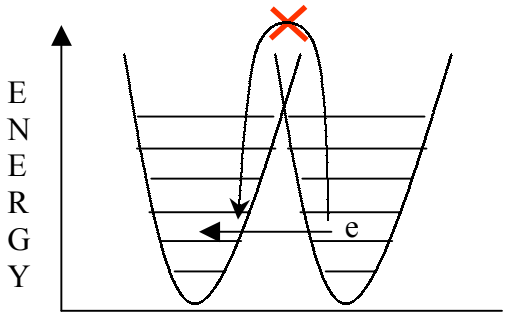

Figure 1.15 Charge Tunnelling.

Most research on charge migration in DNA deals with the process of a hole, or positive ion, transfer. This typically involves electron transfer from the hole acceptor to the positively charged hole donor, which becomes electronically excited. As seen with electrochemical measurements, DNA contains the three electroactive bases adenine, guanine, and cytosine. Guanine has the lowest oxidation potential and therefore is the most stable location on DNA for a hole to reside. Tunnelling, often called in the literature G-tunnelling or G-hopping, is a one-step hole transfer process between localized donor and acceptor sites on the bases[59]. This off-resonant super-exchange is demonstrated in Figure 1.15 where instead of overcoming a high energy barrier to transfer the charge, it "tunnels" from one site to another where energy loss depends on the distance of the charge transfer[60]. Tunnelling is thought to occur primarily from guanine to guanine since it has the lowest oxidation potential,

separated from the next higher base adenine by 0.4 eV[61]. In cases of charge tunnelling or charge hopping, the positive charge will be primarily located on the guanines due to this energy difference.

Charge hopping is thought to occur in two ways. The first mechanism is described in the literature as hopping between delocalized states, however, the description given is more characteristic of resonant tunnelling. In order to obtain delocalized states over the DNA molecule, the strands of DNA must be synthesized with repeating units of the same nucleotide, and the complementary strand with the base's complement. By using this repeating unit, the π-stacking is more ordered, allowing the orbitals to overlap yielding delocalization. This type of DNA behaves as molecular band conduction[49]. The second type of charge hopping occurs between adjacent nucleotides with similar energies where the charge is temporarily localized. This may occur between base pairs within the double helix or within a single strand between adenine, thiamine, and cytosine. Since these three bases are at a higher energy than guanine (by 0.4-0.7 eV), the charge will hop quickly along the DNA chain until it reaches a lower energy position at guanine. This second form of hopping is also referred to in the literature as A-hopping.

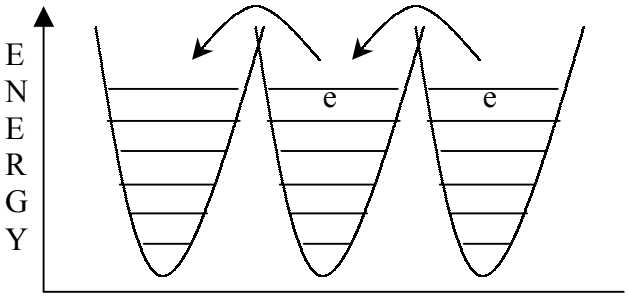

Figure 1.16 Charge Hopping.

A recent study of hole transfer through DNA by hopping and tunnelling demonstrates the efficiency of charge transfer[60]. Electron transfer was initiated by photolysis of a 4'-acylated nucleotide, which is located at the 3' end of the C-A strand.

This photolysis generates a sugar radical cation that injects a positive charge in G_{22} creating a guanine radical cation. This guanine radical cation is either trapped irreversibly by water or stimulates electron transfer through the DNA until electron transfer in halted by the GGG, which is a very stable hole acceptor. The DNA is then treated with piperidine to allow the strand cleavage product containing the radioisotope ^{32}P. Charge transfer efficiency was analyzed by examining the ratio of $^{32}P_{GGG}/^{32}P_{G22}$. The efficiency of charge transfer decreased 8-fold when the guanines were separated by 3 thiamines compared to 1 thiamine, indicating charge tunnelling from one guanine to another. Hopping is thought to occur when the guanines are separated by more than three adenines since there is negligible loss of charge with increasing number of adenine-thiamine base pairs. When more A-T base pairs are added there is little change in charge transfer efficiency (Figure 1.17)[60]. Similar results were found in a study by Ratner et al.[58] These results support the theories of charge hopping and tunnelling.

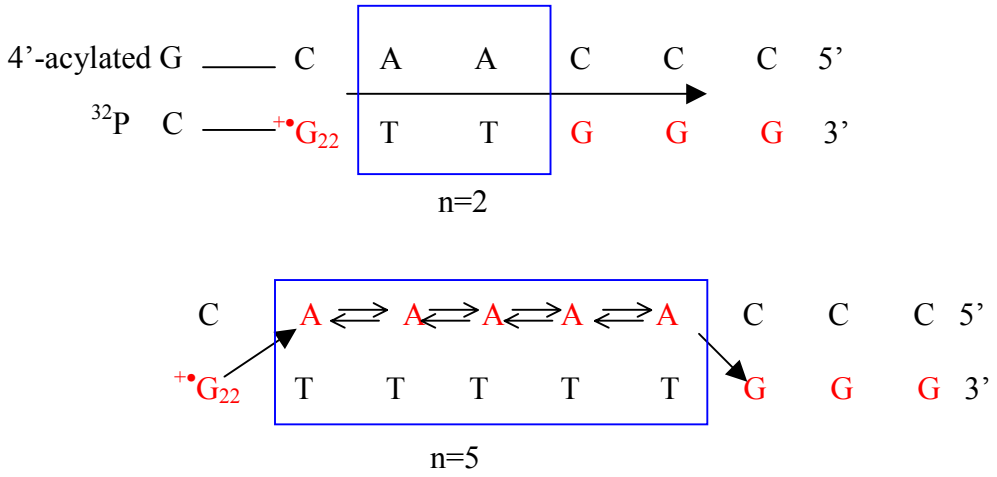

Figure 1.17 Research Results Supporting Theory of Charge Hopping and Tunnelling. Tunnelling occurs for n=0-3; hopping occurs for n≥3.

1.2.5 Photoelectrochemistry and Dye Sensitization

Photoelectrochemistry is the process of converting radiation energy to electrical or chemical energy. The history of Photoelectrochemistry began in 1839 when E. Bequerel discovered a photovoltaic effect while illuminating a platinum electrode covered with silver halide in an electrochemical cell[62]. Materials of certain electrodes absorb photons when irradiated with light, producing an electrical current, or photocurrent. This photocurrent depends on the wavelength of light, electrode potential, and solution composition[63]. Most studies of photoelectrochemical reactions have been done on semiconductor surfaces since they contain a band gap (Figure 1.18), allowing photons to be converted into electrons more easily than in solid metals. When photons are used to excite an electron into the conduction band of a semiconductor, the high

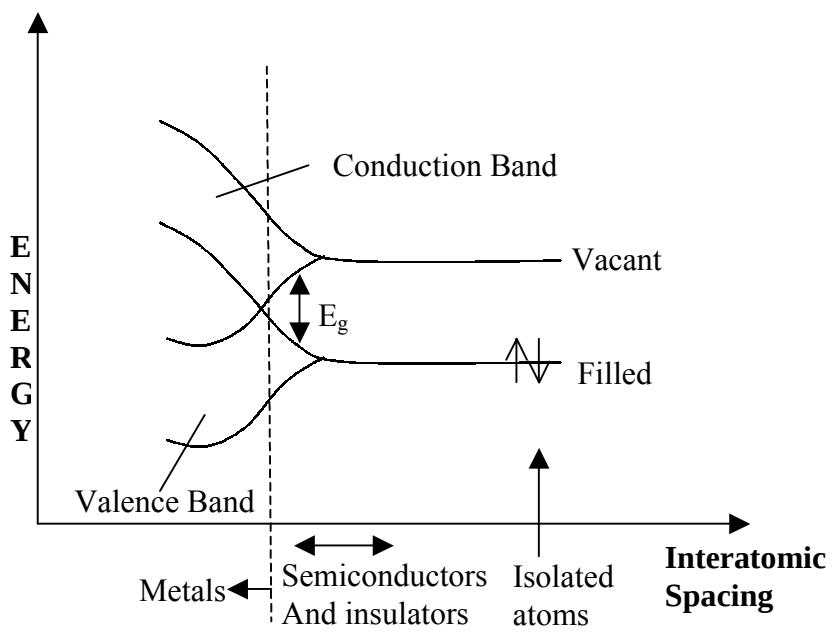

Figure 1.18 Formation of Bands in Solids.

energy level gives it a driving force to allow the electron to flow through the external circuit. When a photon excites an electron in metals, there is no driving force since the valence band and conduction band energies overlap. Figure 1.19 demonstrates how an n-type semiconductor regenerative (no net chemical change in the electrolyte) photoelectrochemical cell works. Typically a semiconductor electrolyte junction is used as the active layer where the electrolyte contains a reducing compound that can replenish the lost electrons in the semiconductor electrode. When a semiconductor is placed in contact with the electrolyte, electronic current initially flows across the junction until electronic equilibrium is reached, where the Fermi energy of the

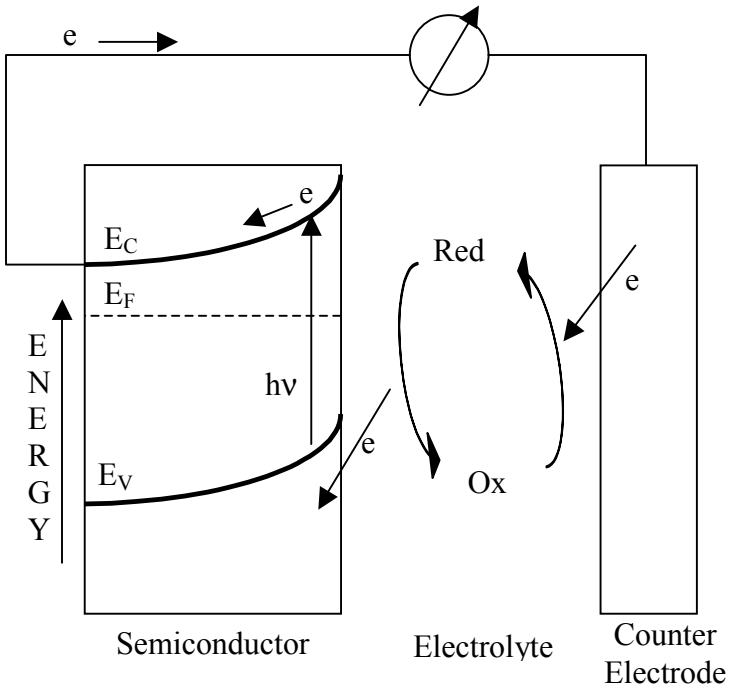

Figure 1.19 n-Type Semiconductor Photoelectrochemical Cell.

electrons in the solid (E_f) is equal to the redox potential of the electrolyte (E_{redox}). Upon illumination, holes in the valence band can oxidize species with a redox potential more

negative than the band edge of the valence band at the interface. The electrons travel from the semiconductor electrode to the metal counter electrode, which is connected via an external load.

Most studies of photoelectrochemical systems focus on semiconductors with a band gap such that efficiently absorbs light from the solar spectrum. Band gaps between 1.1 and 1.7 eV (1100-700nm) are favorable for this. Adsorbing or covalently attaching a photoactive dye to the electrode surface sensitizes the electrode to visible light and produces a photocurrent under irradiation with light of smaller energy than that corresponding to the semiconductor band gap[64]. In other words, dye sensitization is the process of immobilizing a photoactive dye to the electrode surface in order to mediate the electron transfer reactions (Figure 1.20).

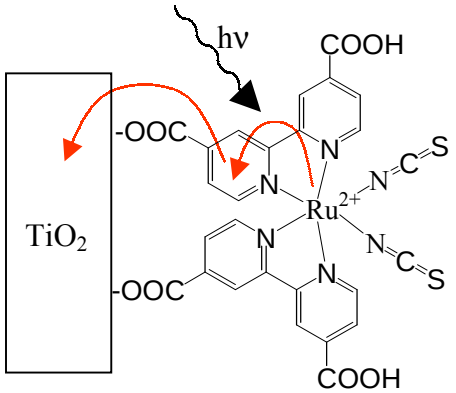

Figure 1.20 Adsorption of the dye.

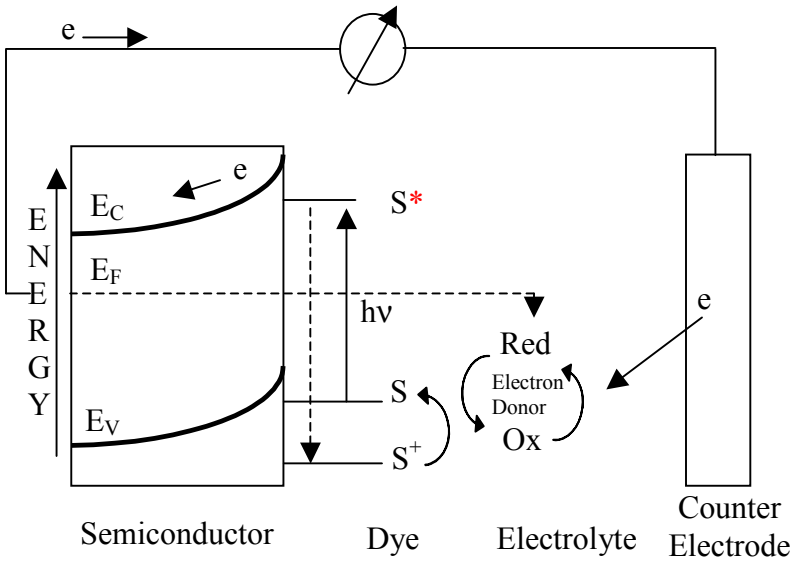

Figure 1.21 Dye Sensitized Semiconductor Photoelectrochemical Cell.

The dye sensitized photoelectrochemical cell (Figure 1.21) works very similar to a regular semiconductor photoelectrochemical cell. The dye absorbs the photon sending an electron from the highest occupied molecular orbital into the excited state. The electron is then injected into the semiconductor electrode where it travels to the counter electrode in the same manner as before. The electrolyte contains a reductant that restores the electron to the dye.

Both photoelectrochemical cells mentioned above have been studied in detail. Since most studies focus on increasing photocurrent efficiency few studies have been performed using metals. As mentioned above, metals do not contain a band gap since the conduction and valence bands of metals overlap (Figure 1.22), therefore they are not as efficient as semiconductors for photoelectrochemistry. This energy level of solids below which all states are full and above which all states are empty at absolute zero temperature is known as the Fermi energy or the Fermi level.

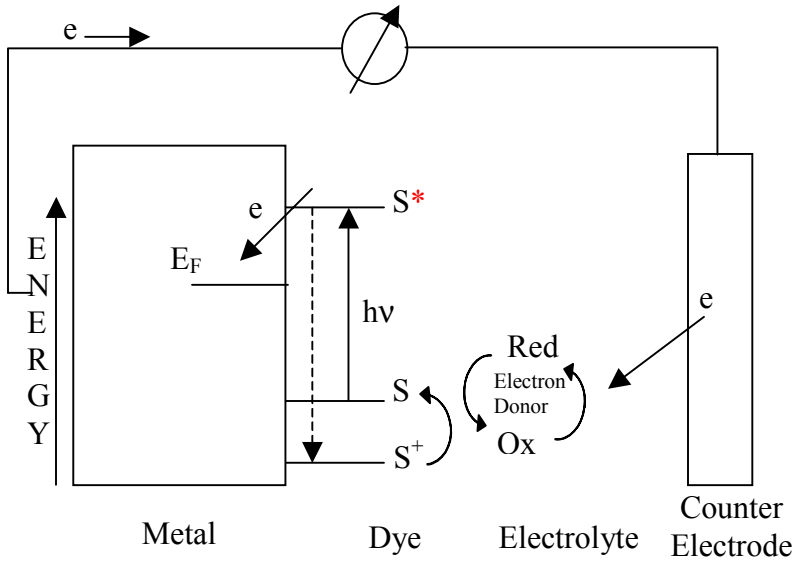

Figure 1.22 Dye Sensitized Metal Photoelectrochemical Cell.

Since the formation of self-assembled monolayers on gold through a gold-sulfur bond are well studied, recent research has taken advantage of this knowledge to characterize the photoactive qualities of molecules on Au rather than a semi-conductor surface[65, 66, 67, 68, 69]. While this system may not be suitable for conversion of photons to energy for human consumption due to its lack in efficiency, it does provide a means of detection for DNA hybridization.

1.2.6 Photoredox-Active Molecule SAMs on Gold

Methods such as Langmuir-Blodgett (LB) techniques and evaporation of molecules onto substrates have allowed electrochemical, photochemical, and optical properties of molecules to be studied. These techniques lead to a physisorbed layer of the compound that is not very stable. For a more stable monolayer the molecule can be chemisorbed to a gold surface through a Au-S linkage which has been well studied[70]. When a thiol is added to the molecule through a long alkane chain (≥10 methyl groups), the molecule can form a well-ordered self-assembled monolayer (SAM) on the gold surface. This has been demonstrated using various compounds. Sakata et al.[71] investigated the photoelectrochemical properties of a C_{60} fullerene by irradiating the 0.48 cm^2 SAM with $\lambda = 403 \pm 6.9$ nm light of 6.6 mW cm^{-2} and +0.1 V bias voltage. An anodic photocurrent of 380 nA cm^{-2} was obtained. Photoelectrochemical properties of porphyrins[72,73,74] and azobenzenes[75,76] have also been studied. Sakata et al.[77] also studied how the length of the alkane chain affects the photocurrent of porphyrins. At $\lambda = 438.5 \pm 4.9$ nm, light intensity of 4.4 mW cm^{-2}, +0.23V bias voltage, and electrode area of 0.57 cm^2 photocurrent increased with the number of carbons ranging from 1 to 10 carbons in

the alkane chain. Another study[74] incorporated ferrocene into the molecule between the porphyrin and thiol, within the alkane chain. The ferrocene acts as an electron transport or relay since the electron transfer of this group is known to be very fast. An increase in photocurrent was observed in comparison to the molecule without the ferrocene. Chain length effects have also been studied with a $[Ru(bpy)_3]^{2+}$ molecule[78] on an electrode area of 0.3 cm^2. Results suggested that the increase in photocurrent with increasing chain length was due to the rate of electron traveling through the alkane chain over distance (Figure 1.23). With longer chain lengths, the rate of electrons from the gold back to the ground-state $[Ru(bpy)_3]^{3+}$ may become slower than the rate of electrons injected into the circuit. Methyl viologen incorporated into the alkane chain to mediate electron transfer[79] demonstrated a visible increase in photocurrent (Figure 1.24).

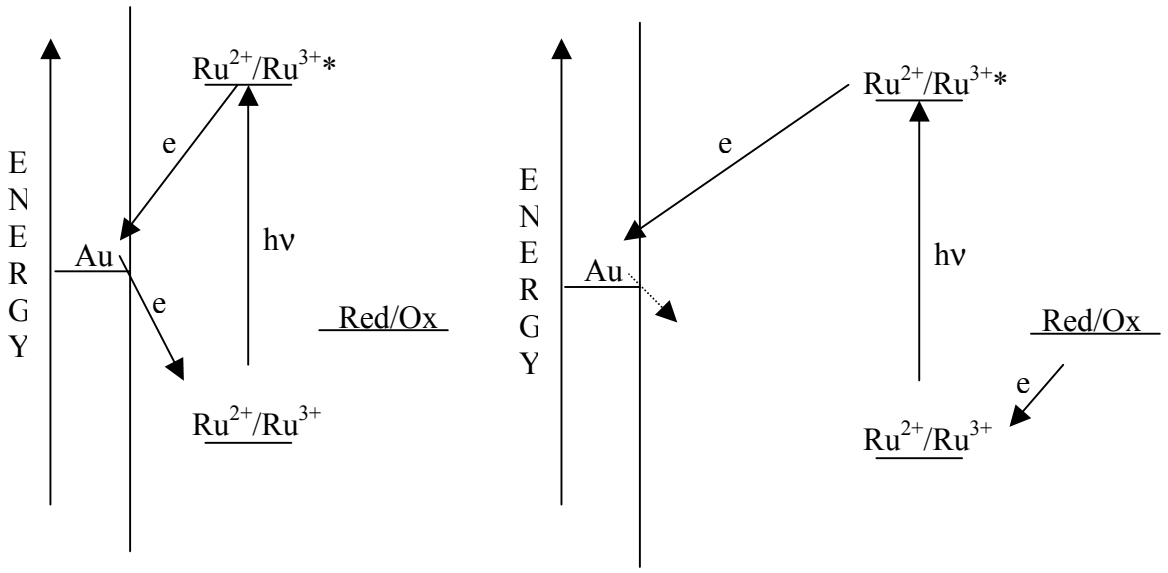

Figure 1.23 Distance Dependence of Photoredox Active Molecule on Photocurrent.

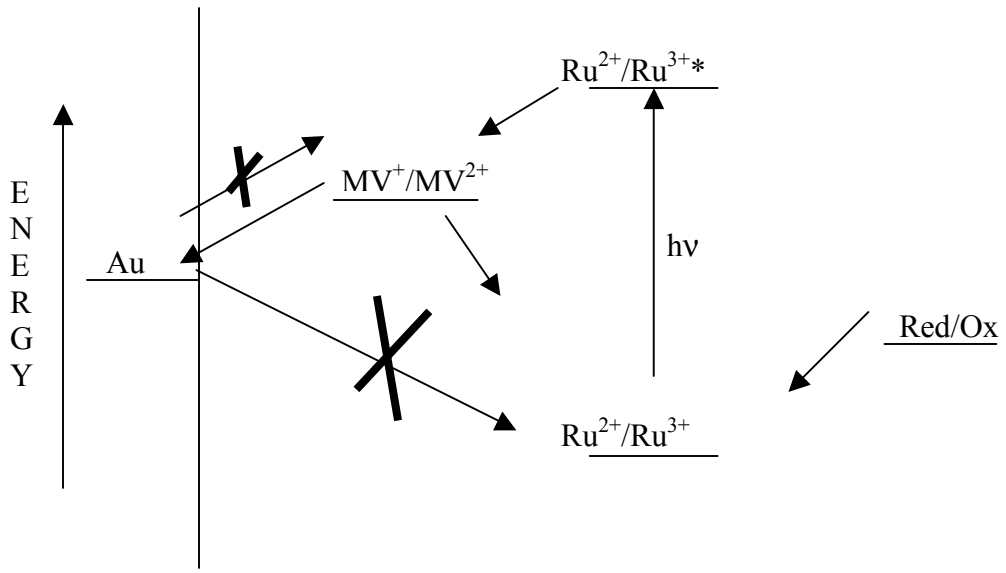

Figure 1.24 Methyl Viologen as Electron Mediator.

1.3 Scope

This thesis focuses on a novel way to detect DNA hybridization for the purpose of its incorporation into DNA microarray technology. Photoelectrochemistry can be used as a detection method by attachment of a dye-sensitizing molecule to the target oligonucleotide. Hybridization of this target to a probe oligo located on a microarray can be detected by scanning a beam of white light across the surface of the array. The hybridization location is noted by an increase in current due to the photoelectrochemical response of the dye.

The introduction and background discussed previous methods used for microarray hybridization detection and contains information that supports the theory of photoelectrochemical detection as a fast, simple, and highly sensitive method of detection. Chapter 2 focuses on the synthesis and characterization of the dye molecule, $[Ru(bpy)_3]^{2+}$. Chapter 3 contains information about the preparation of the target and probe oligonucleotides. Chapter 4 discusses the photoelectrochemical response obtained using the dye-sensitized molecule for detection.

1.4 References

[1] Southern, EM. Detection of specific sequences among DNA fragments separated by gel electrophoresis. *J. Mol. Biol.* **1975**, 98 (3) 503-517.

[2] Wang, J., Rivas, G., Cai, X., Palecek, E., Nielsen, P., Shiraishi, H., Dontha, N., Luo, D., Parrado, C., Chicharro, M., Farias, P.A.M., Valera, F.S., Grant, D.H., Ozsoz, M., and Flair, M.N. DNA electrochemical biosensors for environmental monitoring. A review. *Analytica Chimica Acta* **1997**, 347, 1-8.

[3] Wang, J., Fernandes, J.R., and Kubota, L.T. Polishable and renewable DNA hybridization biosensors. *Anal. Chem*. **1998**, 70, 3699-3702.

[4] http://www.thetech.org/exhibits_events/online/genome/DNA5.html

[5] www.gene-chips.com

[6] a) Schena, M. DNA Microarrays – A Practical Approach. *Oxford University Press* **1999**, Chapter 1.

[7] Schena, M, Heller, R.A., Theriault, T.P., Konrad, K., Lachenmeier, E., and Davis, R.W. Microarrays: biotechnology's discovery platform for functional genomics. *Tibtech.* **1998**, 16, 301-306.

[8] http://www.science.nus.edu.sg/Research/News/Jun2000/huanglq/html

[9] Palanti, S., Marrazza, G., and Mascini, M. Electrochemical DNA Probes. *Analytical Letters* **1996**, 29, 2309-2331.

[10] Palecek, E. Electrochemical behaviour of biological macromolecules. *Bioelectrochemistry and Bioenergetics* **1986**, 15, 275-295.

[11] Korri Youssoufi, H., Garnier, F, Srivastava, P, Godillot, P., and Yassar, A. Toward bioelectronics: specific DNA recognition based on an oligonucleotide-funtionalized polypyrrole. *J. Am. Chem. Soc.* **1997**, 119, 7388-7389.

[12] Napier, M.E., Loomis, C.R., Sistare, M.F., Kim, J., Eckhardt, A.E., and Thorp, H.H. Probing biomolecule recognition with electron transfer: electrochemical sensors for DNA hybridization. *Bioconjugate Chem*. **1997**, 8, 906-913.

[13] Armistead, P.M., and Thorp, H.H. Modification of indium tin oxide electrodes with nucleic acids: detection of attomole quantities of immobilized DNA by electrocatalysis. *Anal. Chem*. **2000**, 72, 3764-3770.

[14] Bardea, A., Patolsky, F., Dagan, A., and Wil;lner I. Sensing and amplification of loigonucleotide-DNA interactions by means of impedance spectroscopy: a route to a Tay-Sachs sensor. *Chem. Commun*. **1999**, 21-22.

[15] Millan, K.M. and Mikkelsen, S.R. Sequence-selective biosensor for DNA based on electroactive hybridization indicators. *Anal. Chem.* **1993**, 65, 2317-2323.

[16] Millan, K.M., Saraullo, A., and Mikkelsen, S.R. Voltammetric DNA biosensor for Cystic Fibrosis based on a modified carbon paste electrode. *Anal. Chem.* **1994**, 66, 2943-2948.

[17] Lee, T.-Y. and Shim, Y.-B. Direct DNA hybridizaton detection based on the oligonucleotide-functionalized conductive polymer. *Anal. Chem.* **2001**, 73, 5629-5632.

[18] Palček, E. and Fojta M. DNA hybridization and damage. *Anal. Chem.* **2001**, 73, 75A-83A.

[19] Yu, C.J., Wan, Y., Yowanto, H., Li, J., Tao, C., James, M.D., Tan, C.L., Blackburn, G.F., Meade, T.J. Electronic detection of single-base mismatches in DNA with ferrocene-modified probes. *J. Am. Chem. Soc.* **2001**, 45, 123.

[20] Umek, R.M. Determination of sequence variations in nucleic acids by electrochemical detection of hybrids using probes labeled with redox groups. *PCT Int. Appl.* **2001, 158** pp.

[21] Takenaka, S., Yamashita, K., Takagi, M., Uto, Y.,and Kondo, H. DNA Sensing on a DNA Probe-Modified Electrode Using Ferrocenylnaphthalene Diimide as the Electrochemically Active Ligand. *Anal. Chem.* **2000**, 72, 1334-1341.

[22] Schena, M. DNA Microarrays – A Practical Approach. *Oxford University Press* **1999**, Chapter 2.

[23] Hames, B.D. and Higgins, S.J. Gene Probes 1 – A Practical Approach. *Oxford University Press* **1995**, Chapter 1.

[24] Thiel, A.J., Frutos, A.G., Jordan, C.E., Corn, R.M., and Smith, L.M. In situ surface plasmon resonance imaging detection of DNA hybridization to oligonucleotide arrays on gold surfaces. *Anal. Chem.* **1997**, 69, 4948-4956.

[25] Lee, H.J., Goodrich, T.T., and Corn, R.M. SPR imaging measurements of 1-D and 2-D DNA microarrays created from microfluidic channels on gold thin films. *Anal. Chem.* **2001**, 73, 5525-5531.

[26] Jordan, C.E., Frutos, A.G., Thiel, A.J, and Corn, R.M. Surface plasmon resonance imaging measurements of DNA hybridization adsorption and streptavidin/DNA

multiplayer formation at chemically modified gold surfaces. *Anal. Chem.* **1997**, 69, 4939-4947.

[27] Gu, J.H., Lü, H., Chen, Y.W., Liu, L.Y., Wang. P., Ma, J.M., and Lu, Z.H. Enhancement of the sensitivity of surface plasmon resonance biosensor with colloidal gold labeling technique. *Suramolecular Science* **1998**, 5, 695-698.

[28] He, L., Musich, M.D., Nicewarner, S.R., Salinas, F.G., Benkovic, S.J., Natan, M.J., and Keating, C.D. Colloidal Au-enhanced surface plasmon resonance for ultrasensitive detection of DNA hybridization. *J. Am. Chem. Soc.* **2000**, 122, 9071-9077.

[29] Reichert, J., Csáki, A. Köhler, J.M., and Fritzsche, W. Chip-based optical detection of DNA hybridization by means of nanobead labeling. *Anal. Chem.* **2000**, 72, 6025-6029.

[30] Niemeyer, C.M., Ceyhan, B., Gao, S., Chi, L, Peschel, S., and Simon, U. Site-selective immobilization of gold nanoparticles functionalized with DNA oligomers. *Colloid Polym. Sci.* **2001**, 279, 68-72.

[31] Taton, T.A., Mirking, C.A., and Letsinger, R.L. Scanometric DNA array detection with nanoparticles probes. *Science* **2000**, 289, 1757-1760.

[32] Taton, T.A., Lu, G., and Mirking, C.A. Two-color labeling of oligonucleotide arrays via size-selective scattering of nanoparticles probes. *J. Am. Chem. Soc.* **2001**, 123, 5164-5165.

[33] Okahata, Y., Matsunobu, Y., Ijiro, K., Mukae, M., Murakami, A., and Makino, K. Hybridization of nucleic acids immobilized on a quartz crystal microbalance. *J. Am. Chem. Soc.* **1992**, 114, 8299-8300.

[34] Okahata, Y, Kawase, M., Niikura, K., Ohtake, F., Furusawa, H, and Ebara Y. Kinetic measurements of DNA hybridization on an oligonucleotide-immobilized 27-MHz quartz crystal microbalance. *Anal. Chem.* **1998**, 70, 1288-1296.

[35] Sastry, Murali, Ramakrishna, V., Pattarkine, M, and Ganesh, K.N. Studies on the formation of DNA-cationic lipid composite films and DNA hybridization in the composites. *J. Phys. Chem. B* **2001**, 105, 4409-4414.

[36] Caruso, F., Furlong, D.N., Niikura, K., and Okahata, Y. In-situ measurement of DNA immobilization and hybridization using a 27 MHZ quartz crystal microbalance. *Colloids Surf. B.* **1998**, 10, 199-204.

[37] Wang, J., Nielsen, P.E., Jiang, M., Cai, X., Fernandes, J.R., Grant, D.H., Ozsoz, M., Beglieter, A, and Mwat, M. Mismatch-sensitive hybridization detectionby peptide nucleic acids immobilized on a quartz crystal microbalance. *Anal. Chem.* **1997**, 69, 5200-5202.

[38] Junhui, Z., Hong, C., and Ruifu, Y. DNA based biosensors. *Biotechnology Advances* **1997**, 15, 43-58.

[39] Iguchi, K. Semiconductivity and band gap of a double strand of DNA. *Journal of the Physical Society of Japan* **2001**, 70, 593-597.

[40] http://www.nature.com/nsu/990408/990408-6.html

[41] Watson, J. and Crick, F. A structure for deoxyribose nucleic acid. *Nature* **1953**, 171, 737.

[42] Eley, D.D. and Spivey, D.I. *Trans. Faraday Soc*. **1962**, 58, 44.

[43] Hall, D.B., Homlin, R.E., and Barton, J.K. Nature, 1996, 382, 731.

[44] Okahata, Y., Kobayashi, T., Nakayama, H., and Tanaka, K. DNA-aligned cast film and its anisotropic electron conductivity. *Supramol. Sci*. **1998**, 5, 317.

[45] Fink. H.W. and Schoenenberger, C. Electrical conduction through DNA molecules. *Nature* **1999**, 398, 407.

[46] Kasumov, A.Yu., Kociak, M., Guéron, S., Reuley, B., Volkov, V.T., Klinov, D.V., and Bouchiat, H. Proximity-induced superconductivity in DNA. *Science* **2001**, 291, 280-282.

[47] Kelley, S.O., Jackson, N.M., Hill, M.G., and Barton, J.K. Long range electron transfer through DNA films. *Angew. Chem., Int. Ed.* **1999**, 38, 941.

[48] Braun, E., Eichen, Y, Sivan, U., and Ben-Yoseph, G. *Nature* **1998**, 391, 775.

[49] Porath, D., Bezryadin, S, de Vries, S., and Dekker, C. Direct measurement of electrical transport through DNA molecules. *Nature* **2000**, 403, 635-638.

[50] Lewis, F.D., Wu, T., Zhang, Y., Letsinger, R.L., Greenfield, S.R., and Wasielewski, M.R. Sistance-dependent electron transfer in DNA hairpins. *Science* **1997**, 277, 673-676.

[51] Harriman, A. Electron tunnelling in DNA. *Angew. Chem., Int. Ed.* **1999**, 38, 945.

[52] Warman, J.M., de Haas, M.P., and Rupprecht, A. DNA: a molecular wire? *Chem. Phys. Lett*. **1996**, 249, 319-322.

[53] Fukui, K. and Tanaka, K. *Angew, Chem., Int. Ed*. **1998**, 37, 158-161.

[54] Larsen, O.F.A., van Stokkum, I.H.M., Gobets, B., van Grondelle, R., and van Amerongen H. Probing the structure and dynamics of a DNA hairpin by ultrafast quenching and fluorescence depolarization. *Biophysical Journal* **2001**, 81, 1115-1126.

[55] Wan, C., Fiebig, T., Kelley, S.O., Treadway, C.R., Barton, J.K., and Zewail, A.H. *Proc. Natl. Acad. Sci. U.S.A.* **1999**, 96, 6014-6019.

[56] Storm, A.J., van Noort, J., de Vries, S., and Dekker, C. Insulating behavior for DNA molecules between nanoelectrodes at the 100 nm length scale. *Applied Physics Letters* **2001**, 79, 3881-3883.

[57] http://www.rnw.nl/science/html/semiconductors200000211.html

[58] Berlin, Y.A., Burin, A.L., and Ratner, M.A. Charge Hopping in DNA. *J. Am. Chem. Soc.* **2001**, 123, 260-268.

[59] Bixon, M., Giese, B., Wessely, S, Langenbacher, T., Michel-Beyerle, M.E., and Jortner, J. Long-range charge hopping in DNA. *Proc. Natl. Acad. Sci.* **1999**, 96, 11713-11716.

[60] Glese, B., Amaudrut, J., Köhler, A.-K., Spormann, M., and Wessely, S. Direct observation of hole transfer through DNA by hopping between adenine bases and by tunnelling. *Nature* **2001**, 412, 318-320.

[61] Steenken, S. and Jovanovic, S.V. How easily oxidizable is DNA? One-electron reduction potentials of adenosine and guanosine radicals in aqueous solution. *J. Am. Chem. Soc.* **1997**, 119, 617-618.

[62] Bequerel, E. *C. R. Des. Scéances Naturelles* **1939**, 9, 561.

[63] Bard, A.J. and Faulkner, L.R. Electrochemical Methods: Fundamentals and Applications. *John Wiley and Sons, Inc.* **2001**, Chapter 18.

[64] Lewis, N.S. Photoelectrochemistry: Energy conversion using semiconductor electrodes. *The electrochemical Society Interface* **1996**, 28-31.

[65] Koide, Y., Terasaki, N., Akiyama, T., and Yamada, S. Effects of spacer-chain length on the photoelectrochemical responses of monolayer assemblies with ruthenium tris(2,2'-bipyridine) – viologen linked disulfides. *Thin Solid Films* **1999**, 350, 223-227.

[66] Kuwahara, Y., Akiyama, T., and Yamada, S. Facile fabrication of photoelectrochemical assemblies consisting of gold nanoparticles and a tris(2,2'-bipyridine)ruthenium(II) – viologen linked thiol. *Langmuir* **2001**, 17, 5714-5716.

[67] Imahori, H., Azuma, T., Ajavakom, A., Norieda, H., Yamada, H., and Sakata, Y. An investigation of photocurrent generation by gold electrodes modified with self-assembled monolayers of C_{60}. *J. Phys. Chem. B.* **1999**, 103, 7233-7237.

[68] Imahori, H., Norieda, H., Ozawa, S., Ushida, K., Yamada, H., Azuma, T., Tamaki, K., and Sakata, Y. Chain length effect on photocurrent from polymethylene-linked porphyrins in self-assembled monolayers. *Langmuir* **1998**, 14, 5335-5338.

[69] Kondo, T., Yanagida, M., Nomura, S., Ito, T., and Uosaki, K. j pH-dependent photoinduced elctron transfer at the gold elctrode modified with a self-assembled monolayer of a porphyrin-mercaptoquinone coupling molecule. *J. Electroanal. Chem.* **1997**, 438, 121-126.

[70] Ulman, A. An introduction to ultrathin organic films form Langmuir-Blodgett to self-assembly. *Academic Press: New York* **1991**.

[71] Imahori, H., Azuma, T., Ajavakom, A., Norieda, H., Yamada, H., and Sakata, Y. An investigation of photocurrent generation by gold electrodes modified with self-assembled monolayers of C60. *J. Phys. Chem. B* **1999**, 103, 7233-7237.

[72] Kondo, T., Ito, T. Nomura, S., and Uosaki, K. Photoelectrochemical characteristics of a self-assembled monolayer of porphyrin-mercaptoquinone coupling molecules. *Thin Solid Films* **1996**, 652, 284-285.

[73] Simpson, T.R.E., Revell, D.J., Cook, M.J., and Russell, D.A. Evanescent wave excited fluorescence from self-assembled phthalocyanine monolayers. *Langmuir* **1997**, 13, 460.

[74] Uosaki, K., Kondo, T., Zang, X.-Q., and Yanagida, M. Very efficient visible light-induced uphill electron transfer at a self-assembled monolayer with a porphyrin-ferrocene-thiol linked molecule. *J. Am. Chem. Soc.* **1997**, 119, 8367.

[75] Ye, Q., Fang. J., and Sun, L. Surface-enhanced raman scattering from functionalized self-assembled monolayers. 2. Distance dependence of enhanced raman scattering from an azobenzene terminal group *J. Phys. Chem. B* **1997**, 101, 8221.

[76] Yu, H.Z., Shao, H.B., Luo, Y., Zhang, H.L., and Liu, Z.F. Evaluation of the tunneling constant for long range electron transfer in azobenzene self-assembled monolayers on gold. *Langmuir* **1997**, 13, 5774.

[77] Imahori, H., Norieda, H., Ozawa, S., Ushida, K., Yamada, H., Azuma, T., Tamaki, K., and Sakata, Y. Chain length effect on photocurrent from polymethylene-linked porphyrins in self-assembled monolayers. *Langmuir* **1998**, 14, 5335-5338.

[78] Koide, Y., Terasaki, N., Akiyama, T., and Yamaka, S. Effects of spacer-chain length on the photoelectrochemical responses of monolayer assemblies with ruthenium tris (2,2'-bipyridine) – viologen linked disulfides. *Thin Solid Films* **1999**, 350, 223-227.

[79] Yamada, S., Koide, Y., and Matsuo, T. A photoresponsive molecular assembly consisting of ruthenium (II) tris(2,2'-bipyridine) – viologen linked disulfide and hexadecanethiol prepared on a gold surface: effect of viologen moity. J. of Electroanal. Chem. 1997, 462, 23-26.

Chapter 2: Synthesis and Characterization of Thiolated $[Ru(bpy)_3]^{2+}$

2.1 Introduction

Tris-2,2'-bipyridyl ruthenium (II) is a molecule that has been studied for decades due to its chemiluminescence and photoelectrochemical properties. While $[Ru(bpy)_3]^{2+}$ has been thoroughly studied in solution, more recently the molecule has been modified for attachment to substrates either through electrostatic interactions[1] or covalent bond[2,3,4] in order to obtain a better understanding of electron transfer within the molecule. Attachment of $[Ru(bpy)_3]^{2+}$ to a substrate may allow the molecule to be incorporated into electronic devices in the near future as research on nanoscale electronics progresses.

The research presented in this thesis focuses on a $[Ru(bpy)_3]^{2+}$ molecule which has been modified by attachment of a thiol to one of the bipyridine ligands via an alkane chain. The addition of this thiol allows the molecule to attach to a gold substrate through a Au-S bond. This thiol can then be used as a marker for the target oligonucleotide by attaching the thiolated $[Ru(bpy)_3]^{2+}$ as well as the target oligo to a gold colloid. This target can then be used for DNA microarrays that use conductive or semiconductive substrates, such as gold or indium tin oxide. After the target hybridizes to the probe DNA, hybridization can be detected using photoelectrochemistry as discussed in Section 1.2.5. This chapter focuses on the synthesis and characterization of this thiolated molecule.

2.2 Experimental

2.2.1 Materials

All chemicals were used as received from vendors without further purification except where noted. 4,4'-dimethyl-2,2'-dipyridyl, lithiumdiisopropylamide (LDA), and potassium thioacetate were supplied by Aldrich. Cis-dichlorobis(2,2'-bipyridine) ruthenium (II) dihydrate [$Ru(Cl)_2(bpy)_2$] was supplied by Strem Chemicals. $Cl_2Ru(bpy)_2$ was further purified by rinsing with water and drying under vacuum. Fisher Scientific supplied sodium perchlorate. Acros supplied 1,5-dibromopentane. Mallinckrodt supplied ammonium chloride. Evaporated Metal Films supplied Gold Slides (1000Å Gold on 50Å Titanium prepared on a glass slide). Tetrahydrofuran (THF) was supplied by various venders and dried over sodium and benzophenone. All solvent used were reagent grade. Purification was monitored by thin layer chromatography on silica gel and nuclear magnetic resonance (NMR).

2.2.2 Synthesis

4-(6-bromohexyl)-4'-methyl-2,2'-dipyridyl (**1**)[5,6,7]. The synthetic procedure of **1** is shown in Figure 2.1. All flasks in the following reaction were kept under argon. 2g of 4,4'-dimethyl-2,2'-dipyridyl (11mmol) was weighed into a dry 250ml roundbottom flask equipped with a stirbar and sealed with a rubber stopper. 50ml of freshly distilled THF was added to the roundbottom using a cannula. Additional THF was added (no more than 20ml) if needed for all of the dipyridyl to dissolve. In a glovebox, 1.4 equivalents of LDA (15mmol) was weighed into a separate dry 250ml roundbottom flask equipped with a stirbar, sealed with a rubber stopper, and removed from the glovebox.

The flask was cooled to -78°C using a bath of dry ice in acetone. 75ml of freshly distilled THF was placed in a clean roundbottom flask, cooled to -78°C, and cannulated slowly to the LDA. The LDA would not dissolve completely with additional THF. The LDA solution was cannulated into the dipyridyl solution dropwise over a 30-minute period as the dipyridyl was cooled to -78°C. The reaction mixture stirred for 2 hours at -78°C and was then cannulated into a roundbottom flask containing 1.8ml 1,5-dibromopentane in 20ml THF at room temperature. The reaction mixture stirred overnight and was quenched with 50ml of 5% ammonium chloride in water. The product was extracted using ethyl ether and dried using a rotary evaporator. Product and dipyridyl starting material were crystallized using petroleum ether at 0°C. The product was further purified by crystallization in acetonitrile at 0°C. Typical yields were 25% of desired product. H^1-NMR spectrum in $CDCl_3$ at 300 MHz (δ, ppm): 1.34 m (2H, chain, 3-CH_2), 1.48 m (2H, chain, 4-CH_2), 1.70 m (2H, chain, 2-CH_2), 1.86 m (2H, chain, 5-CH_2), 2.44 s (3H, 4-CH_3), 2.70 t (2H, chain, 1-CH_2), 3.40 t (2H, chain, 6-CH_2), 7.13 d (2H, dipyridyl, $H^{5,5'}$), 8.23 s (2H, dipyridyl, $H^{3,3'}$), 8.55 m (2H, dipyridyl, $H^{6,6'}$).

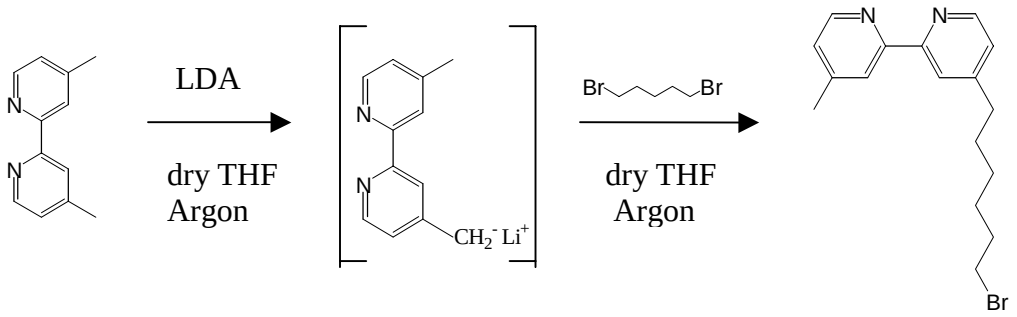

Figure 2.1 Synthesis Scheme for 4-(6-bromohexyl)-4'-methyl-2,2'-dipyridyl.

4-(6-thioacetylhexyl)-4'-methyl-2,2'dipyridyl (**2**)[6,7]. The synthetic procedure of **2** is shown in Figure 2.2. 530mg **1** (1.6mmol) was combined with a 1 equivalent of potassium thioacetate in DMSO under argon and heated to 70°C for 10 hours. DMSO was removed using dropper-to-dropper distillation. The reaction mixture was re-suspended in dichloromethane and washed with water. The reaction yielded 100% desired product. H^1-NMR spectrum in $CDCl_3$ at 300 MHz (δ, ppm): 1.385 m (4H, chain, 3,4-CH_2), 1.715 m (2H, chain, 2-CH_2), 1.856 m (2H, chain, 5-CH_2), 2.318 s (3H, chain, 8-CH_3), 2.439 s (3H, 4'-CH_3), 2.687 t (2H, chain, 1-CH_2), 2.857 t (2H, chain, 6-CH_2), 7.120 d (2H, dipyridyl, $H^{5,5'}$), 8.216 s (2H, dipyridyl, $H^{3,3'}$), 8.530 m (2H, dipyridyl, $H^{6,6'}$).

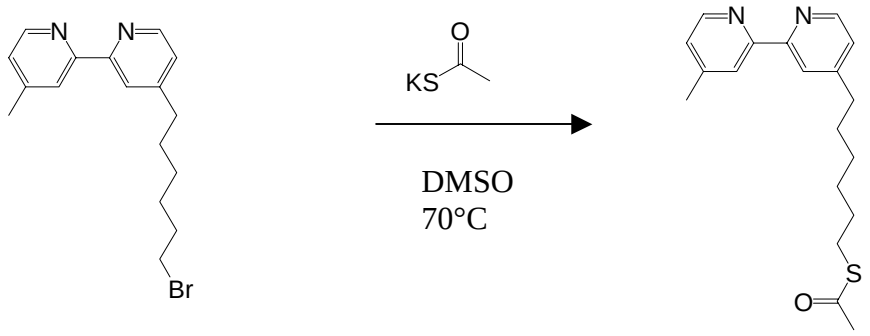

Figure 2.2 Synthesis Scheme for 4-(6-thioacetylhexyl)-4'-methyl-2,2'dipyridyl.

Bis(2,2'bipyridyl)-4-(6-thioacetylhexyl)-4'-methyl-2,2'-dipyridyl ruthenium dichloride (**3**). The synthetic procedure of **3** is shown in Figure 2.3. 500mg of compound **2** was refluxed with 0.9 equivalents of cis-dichlorobis(2,2'-dipyridyl) ruthenium (II) dihydrate in ethanol at 100°C for 4 hours. Ethanol was removed by rotary

evaporation and the reaction mixture was re-suspended in water. Excess compound **2** was extracted from the mixture using dichloromethane. The reaction yielded 99% desired product. H^1-NMR spectrum in D_2O at 300 MHz (δ, ppm): 1.239 m (4H, chain, 3,4-CH_2), 1.438 m (2H, chain, 2-CH_2), 1.665 m (2H, chain, 5-CH_2), 2.226 s (3H, chain, 8-CH_3), 2.554 s (3H, 4'-CH_3), 2.683 t (2H, chain, 1-CH_2), 2.814 t (2H, chain, 6-CH_2), 7.240 m (2H, 4'-methyl-2,2'-dipyridyl, $H^{5,5'}$), 7.399 t (4H, 2,2'-dipyridyl, $H^{5,5'}$), 7.652 m (2H, 4'-methyl-2,2'-dipyridyl, $H^{3,3'}$), 7.855 d (4H, 2,2'-dipyridyl, $H^{3,3'}$), 8.067 t (4H, 2,2'-dipyridyl, $H^{4,4'}$), 8.413 d (2H, 4'-methyl-2.2'-dipyridyl, $H^{6,6'}$), 8.550 d (4H, 2,2'-dipyridyl, $H^{6,6'}$).

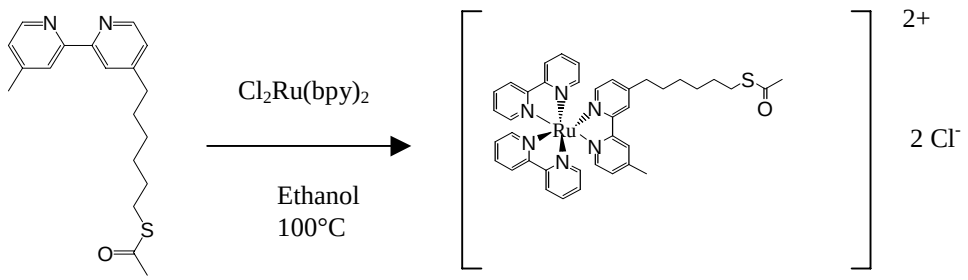

Figure 2.3 Synthesis Scheme for Bis(2,2'bipyridyl)-4-(6-thioacetylhexyl)-4'-methyl-2,2'-dipyridyl ruthenium dichloride.

Counter Ion Exchange

The chloride counter ions on compound 3 may cause oxidative damage to the gold substrate used in the following experiments. In order to reduce this risk, the chloride ions were exchanged with 2 NO_3^- which includes and intermediate step of ion exchange to 2 PF_6^-.

Compound 3 was suspended in a small amount of water. 1M aqueous KPF_6 was added to the compound while stirring. Bis(2,2'bipyridyl)-4-(6-thioacetylhexyl)-4'-methyl-2,2'-dipyridyl ruthenium dihexafluorophosphate precipitated out of solution immediately and was collected on a frit. The compound was rinsed with cold water and ethyl ether. Approximately 30% of the compound was lost during this process. The compound was dried under vacuum and dissolved in acetone. 1M tetrabutyl ammonium nitrate in acetone was added to the compound while stirring. Bis(2,2'bipyridyl)-4-(6-thioacetylhexyl)-4'-methyl-2,2'-dipyridyl ruthenium dinitrate crashed out of solution immediately and was collected on a frit. The compound was rinsed with cold acetone. Approximately 60% of the compound was lost during this procedure.

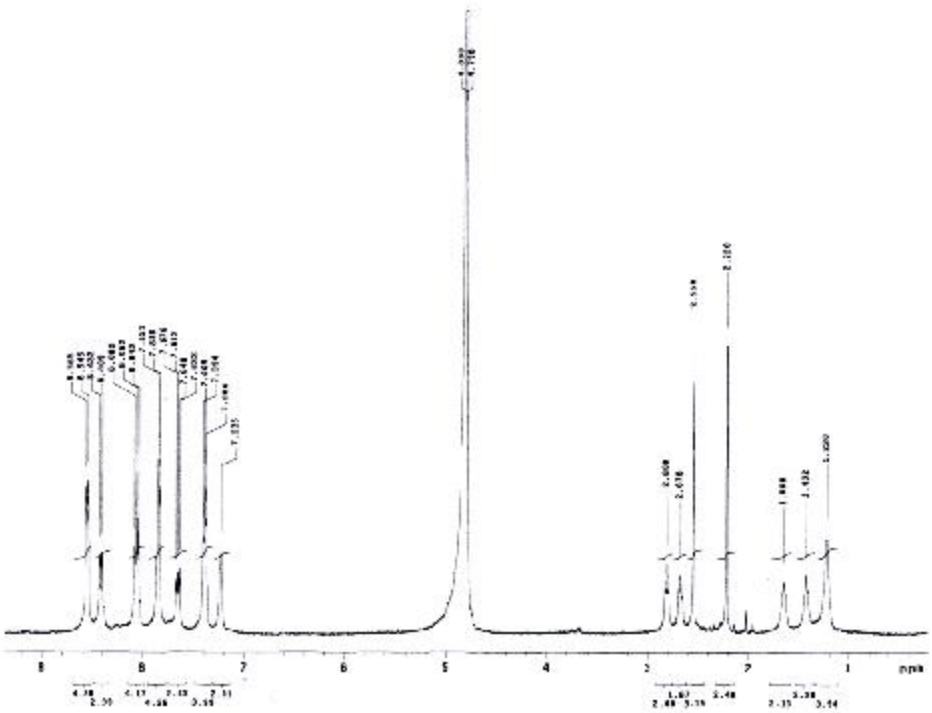

Figure 2.4 NMR Spectrum of Compound 3.

2.2.2 Instrumental Setup

Nuclear Magnetic Resonance. ^{1}H NMR was obtained using either a Varian Mercury 300 MHz or 400 MHz Spectrometer. Both instruments are operated using SUN Ultra 5/360 Workstation software and are equipped with a variable temperature module and a 5 mm PFG Autoswitchable 4N Probe (^{1}H, ^{19}F, ^{13}C, ^{31}P).

Cyclic Voltammetry. Cyclic Voltammetry was used for the characterization of the thiolated $[Ru(bpy)_3]^{2+}$ molecule. An EG&G Princeton Applied Research Potentiostat/Galvanostat Model 273A equipped with EG&G Instruments, Inc. Model 270/250 Research Electrochemistry Software 4.00 was used for all electrochemical measurements. For molecule characterization cyclic voltammetry was performed using a platinum working and counter electrodes and a Ag/AgCl reference electrode at a scan rate of 100 mV/s. The electrolyte was 0.1M tetrabutyl ammonium perchlorate in acetonitrile. The sample was purged for 15 minutes with nitrogen before analysis.

Optical Absorption and Emission Spectral Measurements. A Hewlett Packard HP 8453 UV-Visible spectometer was used with HP Chemstation software. The optical density (OD) of $[Ru(bpy)_3]^{2+}$ was monitored at 450 nm. A quartz cuvette with a 0.5 cm pathlength was used for all measurements.

The emission spectra were obtained using a Photon Technology International (PTI) Fluorometer equipped with a PTI 814 Photomultiplier Detection System. TimeMaster Version 1.2 software distributed by PTI was used to run the instrument and collect data.

X-ray Photoelectron Spectroscopy. XPS data was obtained using a Riber LAS 2000 Surface Analysis System located at the Analytical Instrumentation Facility at North Carolina State University Centennial campus. This instrument is equipped with a cylindrical mirror analyzer and a MAC2 analyzer with Mg Kα X-rays (model CX 700 (Riber source) (1253.6 eV). Resolution for the surface scan was 2 eV and for elemental scans was 1 eV.

2.3 Results and Discussion

2.3.1 Cyclic Voltammetry

A typical cyclic voltammogram of $[Ru(bpy)_3]^{2+}$ in solution shows four reversible, one-electron transfers as demonstrated in Figure 2.5 which are independent of solvent (for acetonitrile, DMSO, DMF, and propylene carbonate). The first redox couple at +1.2 V (vs. Ag/Ag+) corresponds to reaction 2.1.

$$[Ru(bpy)_3]^{3+} + e- \rightleftharpoons [Ru(bpy)_3]^{2+} \qquad (2.1)$$

The three redox couples at –1.3 V, -1.5 V, and –1.7 V correspond to equations 2.2, 2.3, and 2.4, respectively.

$$[Ru(bpy)_3]^{2+} + e- \rightleftharpoons [Ru(bpy)_3]^{1+} \qquad (2.2)$$

$$[Ru(bpy)_3]^{1+} + e- \rightleftharpoons [Ru(bpy)_3]^{0} \qquad (2.3)$$

$$[Ru(bpy)_3]^{0} + e- \rightleftharpoons [Ru(bpy)_3]^{1-} \qquad (2.4)$$

A fourth reduction wave (not shown in Figure 2.4) occurs at a potential more positive of 2.0 V. This reduction is irreversible and is thought to correspond to irreversible decomposition of $[Ru(bpy)_3]^{2-}$ followed by further reduction of the freed ligand[8].

A cyclic voltammogram of the thiolated $[Ru(bpy)_3]^{2+}$ was compared to the unthiolated compound in solution. The counter ions of each compound were exchanged with PF_6^- as outlined in Section 3.3.4 of this thesis. The redox potentials of the thiolated

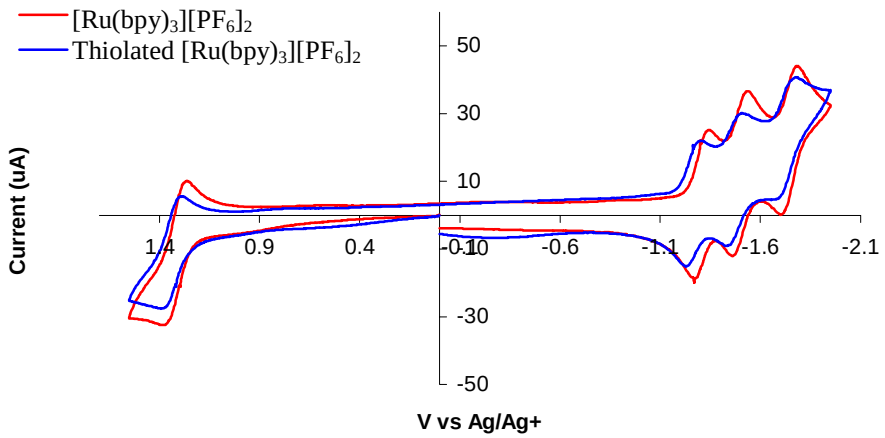

Figure 2.5 Cyclic Volammetry (Pt counter and working electrodes, 0.1M TBAP in CH_3CN) of the two complexes at ~ 1M to demonstrate shift in E°´.

compound was shifted slightly to more positive potentials in comparison to the unthiolated compound.

A cyclic voltammogram of the thiolated $[Ru(bpy)_3]^{2+}$ self-assembled monolayer on a gold surface was unattainable due limitations of gold as a working electrode. The redox potential at +1.2 V vs. Ag/Ag+ was of interest due to its importance in photoelectrochemical measurements as well as confirmation that the thiolated $[Ru(bpy)_3]^{2+}$ was covalently bound to the gold surface. As seen in Figure 3.5, gold begins reduction to gold oxide at a potential of +0.9 V (varies slightly with solvent and

electrolyte) which creates a large anodic current which masks the Ru^{2+}/Ru^{3+} redox potential. XPS was employed to confirm thiol deposition.

2.3.2 Optical Absorption and Emission Spectral Measurements

$[Ru(bpy)_2]^{3+}$ is a d^6 transition metal complex with octahedral geometry. Figure 2.6 shows a simplified molecular orbital diagram of $[Ru(bpy)_2]^{3+}$ along with the ground state absorption spectrum. The d-orbitals, which are mostly localized on the metal, are split into three lower (t_{2g}) and two higher (2_g) orbital energy levels due to the bpy-ligands. Several bands appear in the absorption spectrum that correspond to different types of electronic transitions between the molecular orbitals in the complex. The two bands at 240 nm and 450 nm are caused by a transition of an electron from a π_M metal orbital to the π_L* ligand orbitals. These transitions are called metal-to-ligand charge transfer (MLCT) bands. Bands at 185 nm and 285 nm correspond to ligand centered (LC) bands which results from a transition from a π_L ligand orbital to a π_L* ligand orbital. The weak peaks at 322 nm and 344 nm are due to metal centered (MC) bands occurring due to a transition from the π_M metal orbital to the σ_M* metal orbital[9].

Figure 2.7 shows the absorption and emission spectra for the thiolated $[Ru(bpy)_2]^{3+}$ in comparison to the unthiolated form. The absorption of the compound shifts with various counter ions. Therefore, the counter ions of $[Ru(bpy)_2]^{3+}$ and $[Ru(bpy)_2]^{3+}$ thiol were exchanged with PF_6^- for comparison of the two compounds. The MLCT absorption band at 450 nm was slightly shifted to the blue for the thiolated compound in comparison to the unthiolated. The compounds were then excited at a

wavelength of 450 nm in order to obtain emission spectra. The emission of the thiolated compound was shifted to the red in comparison to the unthiolated compound.

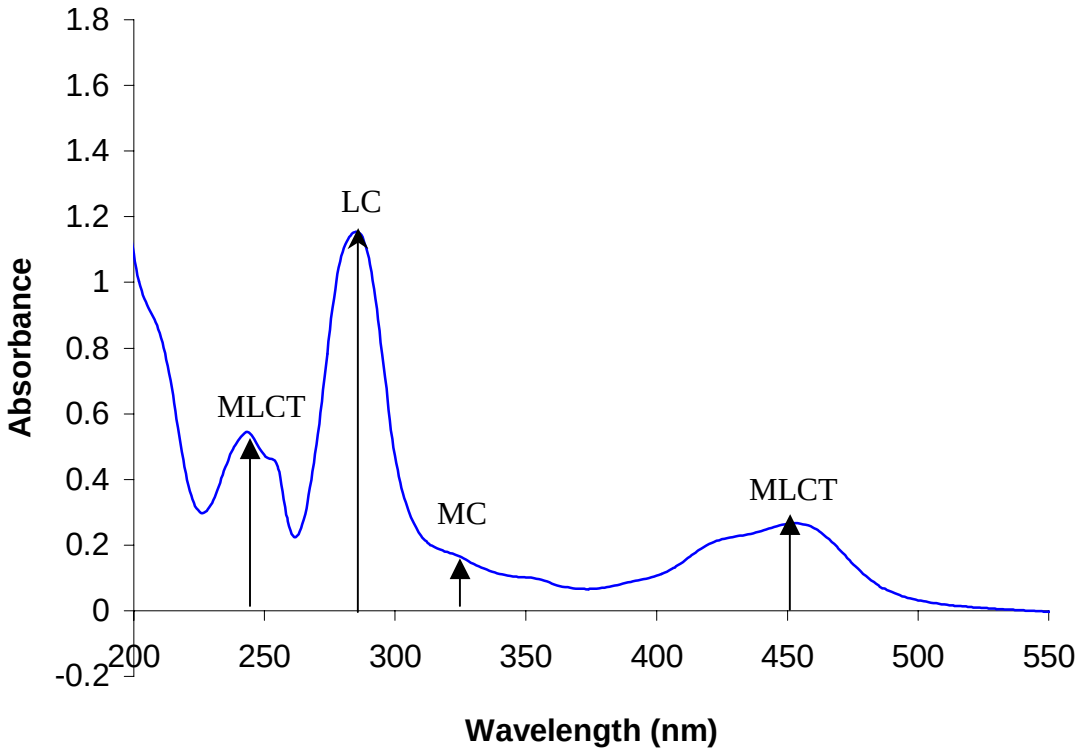

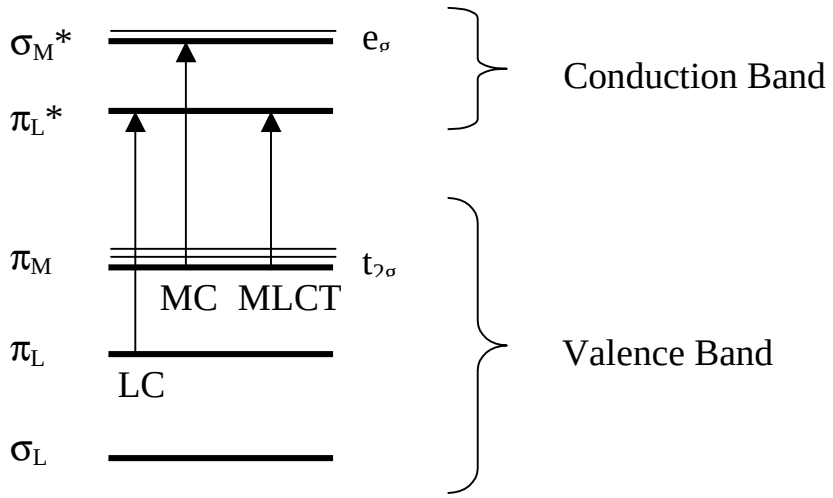

Figure 2.6 Absorption spectrum of $[Ru(bpy)_3]^{2+}$ $2Cl^-$ (in water) together with a schematic molecular orbital diagram. Metal-to-ligand charge transfer (MLCT), ligand centered bands (LC), and metal centered bands (MC).

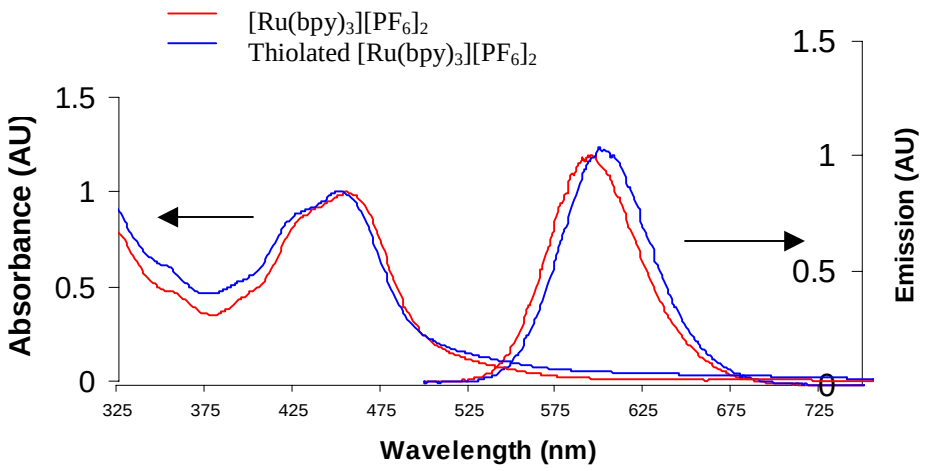

Figure 2.6 Absorption and emission spectra (excitation wavelength = 450nm) of two complexes as their PF_6^- salts in CH_3CN solution at 25°C.

2.3.3 X-ray Photoelectron Spectroscopy

X-ray Photoelectron Spectroscopy (XPS) was used to determine if a self-assembled monolayer (SAM) of the thiolated $[Ru(bpy)_3]^{2+}$ formed on the gold surface since cyclic voltammetry was unable to produce results. The gold slide was cleaned in piranha (30% hydrogen peroxide (35% in water) and 70% sulfuric acid v/v), rinsed with deionized water and dried under nitrogen. The gold slide was then placed in a 1μM aqueous solution of the thiolated $[Ru(bpy)_3]^{2+}$ for 24 hours. The slide was removed, rinsed with deionized water, and dried using nitrogen. The sample was then ready for XPS analysis.

The surface scan of the $[Ru(bpy)_3]^{2+}$ SAM is shown in Figure 2.7. Due to the low concentration of a single layer of the molecule on the gold substrate, only Au, C, and O

are visible in the surface scan. The C and O are from residual H_2O and CO in the XPS vacuum chamber.

An elemental scan was performed in the sulfur $2p_{3/2}$ region as well as the ruthenium $3d_{5/2}$ to confirm the presence of a $[Ru(bpy)_3]^{2+}$ monolayer. The elemental sulfur scan (Figure 2.8) yielded three peaks at 155, 163, and 169eV. The peak at 163eV is attributed to the thiolated sulfur. The shifts in binding energy to 155 and 169eV are due to beam-induced damage of the thiol surface[10]. The peak at 169eV is thought to be a result of sulfate or sulfite that formed as a reaction between the sulfur and H_2O and CO, which can be found in the vacuum chamber as residual gases. The low binding energy sulfur, which formed a large peak at 155eV, is thought to be a more reduced form of the thiolate. The elemental scan of ruthenium and carbon (Figure 2.9) shows a slight positive shift in binding energy for both elements from the text book values (listed in the figure caption). These minor shifts in binding energy are likely due to a calibration error in the instrument.

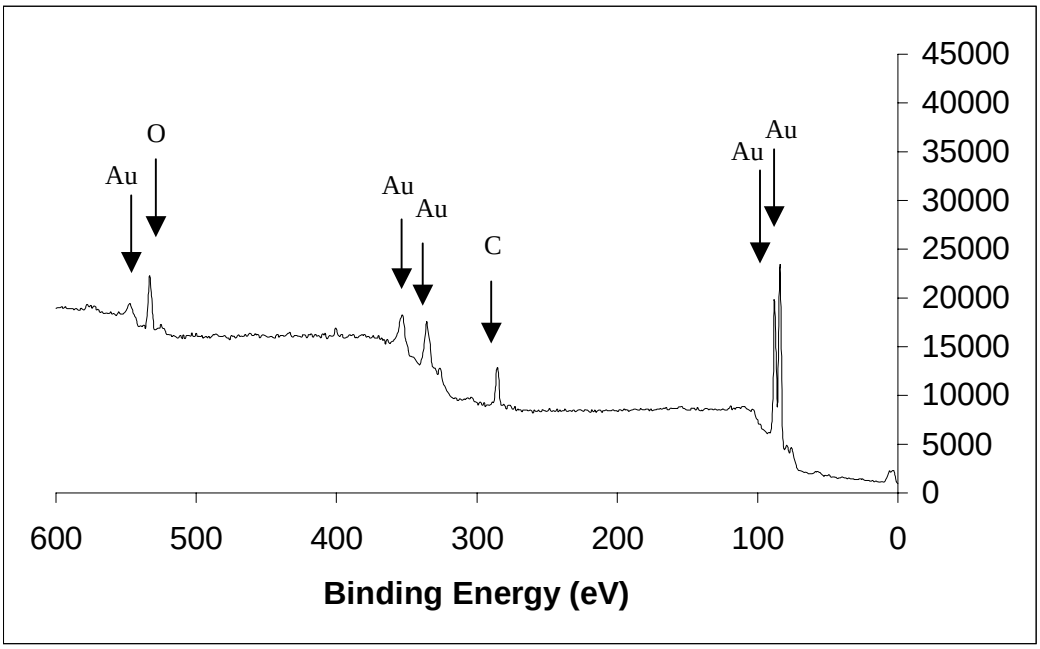

Figure 2.7 XPS Surface Scan Ruthiol modified Gold Slide.

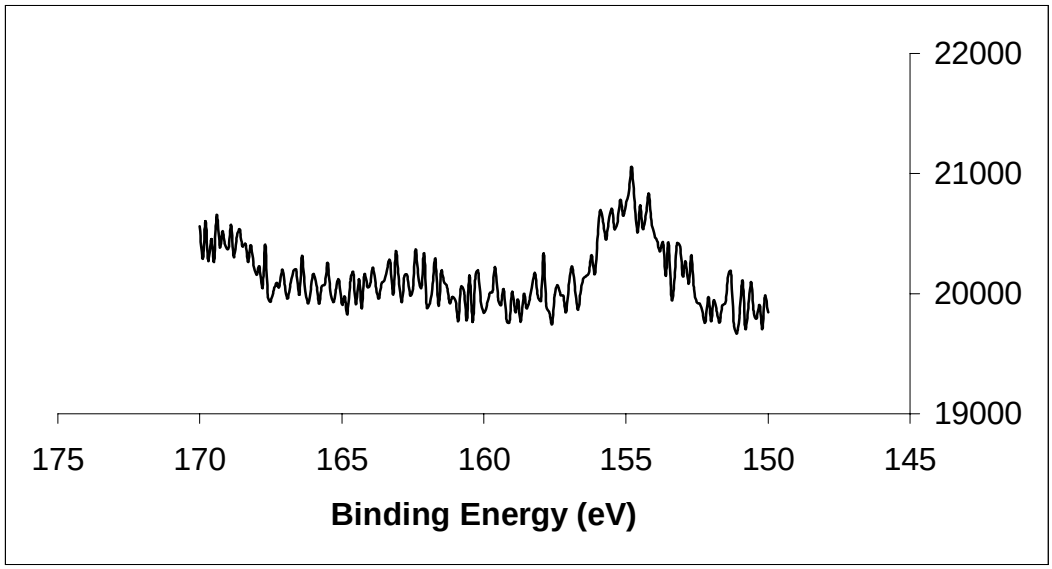

Figure 2.8 XPS Elemental Scan of Sulfur Region ($2p_{3/2}$ = 164.0 eV).

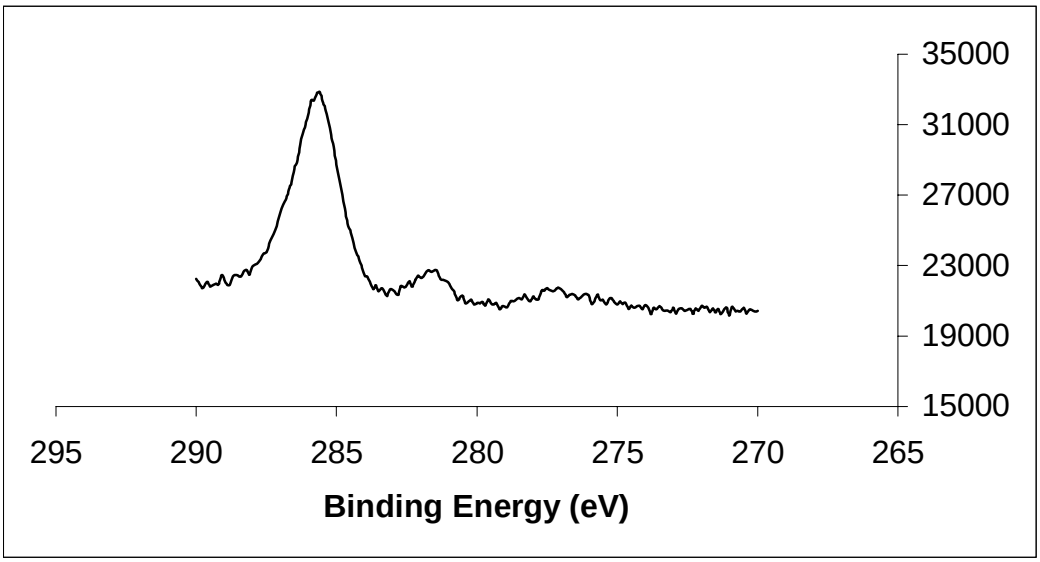

Figure 2.9 XPS Elemental Scan of Carbon (1s = 284.5 eV) and Ruthenium ($3d_{5/2}$ = 280.1 eV) Region.

2.4 References

[1] Lahav, M., Heleg-Shabtai, V., Wasserman, J., Katz, E., Willner, I., Dürr, H., Hu, Y.-Z., and Bossmann, S.H. Photoelectrochemistry with integrated with integrated photosensitizer-electron acceptor and Au-nanoparticle arrays. *J. Am. Chem. Soc.* **2000**, 122, 11480-11487.

[2] Kuwahara, Y., Akiyama, T., and Yamada, S. Construcion of gold nanoparticles-ruthenium (II) tris(2,2'-bipyridine) self-assembled multistructures and their photocurrent responses. *Thin Solid Films* **2001**, 393, 273-277.

[3] Sato, Y. and Uosaki, K. Electrochemical and electrogenerated chemiluminescence properties of tris(2,2'-bipyridine)ruthenium(II)-tridecanethiol derivative on ITO and gold electrodes. *J. Electroanal. Chem.* **1995**, 384, 57-66.

[4] Yamada, S., Koide, Y., and Matsuo, T. A photoresponsive moleculear assembly consisting of ruthenium(II)tris(2,2'-bipyridine)-viologen linked disulfide and hexadecanethiol prepared on a gold surface: effect of viologen moiety. *J. Electroanal. Chem.* **1997**, 426, 23-26.

[5] Ciana, L.D., Hamachi, I., and Meyer, T.J. Synthesis of side-chain derivatives of 2,2'-bipyridine. *J. Org. Chem*. **1989**, 54, 1731-1735.

[6] Maier, V.É. and Shafirovich, V.Ya. Synthesis of photsensitizer pairs containing $Ru(bpy)_3^{2+}$ and an electron acceptor (viologen) linked by a hydrocarbon chain. *Institute of Chemical Physics, Academy of Sciences of the USSR, Chernogolovka Branch*, **1998**, 3, 700-703.

[7] Yamada, S., Koide, Y., Matsuo, T. A photoresponsive molecular assembly consisting of ruthenium (II) tris(2,2'-bipyridine)-viologen linked disulfide and hexadecanethiol prepared on a gold surface: effect of viologen moiety. *J. Electroanal. Chem.* **1997**, 426, 23-26.

[8] Seddon, E.A. and Seddon, K.R. The Chemistry of Ruthenuim. *Elsevier Science Publishers B.V.*, **1984**.

[9] Kalyanasundaram, K. Photochemistry of polypridine and porphyrine complexes. *Academic Press: London* **1992**.

[10] Murty, K.V.G.K., Venkataramanan, M., and Pradeep, T. Self-assembled monolayers of 1,3-benzenedimethanethiol on polycrystalline silver and gold films: an investigation of structure, stability, dynamics, and reactivity. *Langmuir* **1998**, 14, 5446-5456.

Chapter 3: Probe and Target Preparation

3.1 Introduction

Deposition of the probe oligonucleotide onto a gold substrate has been well studied over the past few years. Two methods have been used in order to obtain a densely packed mixed monolayer of the oligonucleotide and 6-mercapto-1-hexanol (MCH) [1]. MCH is used to prevent the negatively charged phosphate backbone of the oligonucleotide from resting on the gold surface. The first method is a sequential method where the thiolated oligonucleotide is first deposited onto the gold substrate. The modified Au substrate is then exposed to an aqueous solution of MCH which deposits onto the gold through a Au-S bond, liberating the electrostatically bound DNA. The second probe deposition method is a co-deposition where the bare gold substrate is exposed simultaneously to the thiolated oligo and MCH. Data reported by Franzen et al.[1] demonstrated that the co-deposition method allows better control over oligo deposition.

Studies involving attachment of the target to gold colloid had also been well studied. This involves stabilizing the sodium citrate-coated Au colloid with bis(p-sulfanoto phenyl) phenyl phosphine (BSPP). Stabilization is necessary since citrate-capped Au colloids are not stable in high salt concentrations, which is crucial for hybridization. The thiolated oligo is then added to the colloid solution. The thiol attaches to the colloid rapidly and is ready for hybridization within an hour.

While the literature preparation for target oligos yields desirable gold-bioconjugates, the preparation for the probe deposition results in a high background signal for the photoelectrochemial technique. This chapter focuses on the preparation of the target oligonucleotide as well as concentrates on optimization of the probe deposition

method in order to obtain the sensitivity required for photoelectrochemical measurements.

3.2 Experimental

3.2.1 Materials

All chemicals were used as received from vendors without further purification except where noted. Dithiothreitol (DTT), triethanolamine, tripropylamine, and triethylamine were supplied by Aldrich. Bis(p-sulfonatophenyl) phenylphosphine dihydrate dipotassium salt (BSPP, Figure 3.2) was supplied by Strem Chemicals. Fisher Scientific supplied disodium ethylenediaminetetraacetic acid (EDTA) and 20 X Saline-Sodium Citrate (20 X SSC). Mallinckrodt supplied potassium phosphate monobasic. Ted Pella, Inc supplied 10nm Gold Colloid. Applied Biosystems, Inc. supplied the oligonucleotides R20 (Linker-AACCAGGATTATCCGCTCAC) and T20 (Linker-GTGAGCGGATAATCCTGGTT) with the linker being a thiol modifier, 1-o-Dimethoxytrityl-hexyl-disulfide, 1'-[(2-cyanoethyl)-(N,N-diisopropyl)]-phosphor amidite (Figure 3.1). Amersham Pharmacia Biotech supplied the PD-10 disposable size exclusion chromatography columns containing Sephadex G-25 Medium. Evaporated Metal Films supplied Gold Slides (1000Å Gold on 50Å Titanium prepared on a glass slide). Tetrahydrofuran (THF) was supplied by various venders and dried over sodium and benzophenone. All solvent used were reagent grade. Purification was monitored by thin layer chromatography on silica gel and nuclear magnetic resonance (NMR).

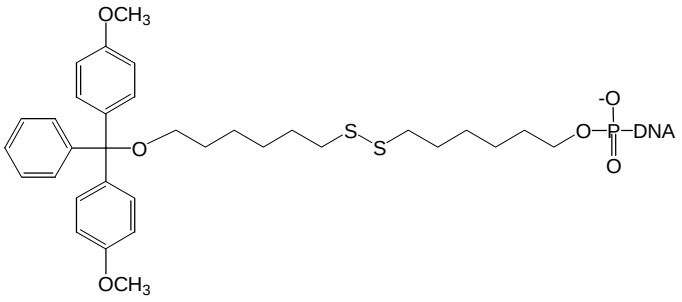

Figure 3.1 C6-Disulfide Linker.

3.2.2 Synthesis

BSPP-capped Gold Nanoparticles. Citrate-capped gold nanoparticles are not stable in aqueous buffers; therefore, bis(p-sulfonatophenyl) phenylphosphine dihydrate dipotassium salt (BSPP) was used to further stabilize the gold nanoparticles[2]. A roundbottom flask and stirbar were cleaned for 10 minutes in aqua regia (75% hydrochloric acid / 25% nitric acid v/v), rinsed with deionized water, and dried in an oven at 120°C. 20ml of 10nm citrate-capped gold colloids (5.7 x 10^{12} particles/ml as determined by BBInternational) were added to the cooled flask and stirred for 5 minutes at room temperature. 24mg BSPP was added to the flask while stirring vigorously. After the reaction stirred at room temperature for 24 hours, the product was purified by addition of salt which causes the product to aggregate. Sodium chloride was added to the solution 50mg at a time (total amount varied from batch to batch) until the solution color changed from red to a bluish-brown. This change in color is due to colloid aggregation in high salt concentrations. The NaCl was allowed to dissolve completely upon each addition since too much NaCl will cause irreversible aggregation. The reaction mixture was pipetted into 1.5ml eppendorf tubes and centrifuged at 14000 RPM for 10 minutes until a reddish-blue pellet formed at the bottom of the tubes. The supernatant containing citrate and excess BSPP was pipetted off and the pellet was re-suspended in 100μl of a 250mg/L aqueous solution of BSPP. Methanol was added dropwise to each of the eppendorf tubes until the solution color changed from

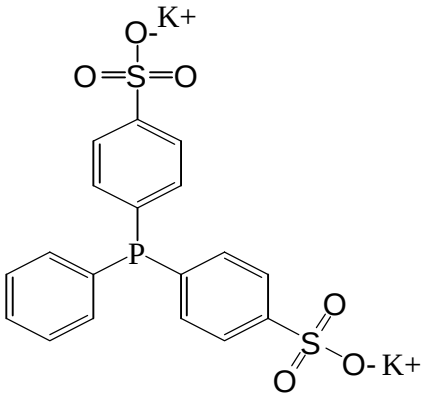

Figure 3.2 BSPP.

red to purple. The colloids were centrifuged at 14000 RPM for 5 minutes, and the supernatant was removed, leaving black pellets in the bottom of the eppendorf tubes. The pellets were dissolved in 250mg/L aqueous BSPP and combined to a final volume of 10ml. The solution was stored at 4°C in a glass vial.

Oligonucleotide Thiol Deprotection and Purification. The oligonucleotides used in the following experiments are purchased with a disulfide linker attached to the 5' end of the oligo. When this oligo is exposed to a gold substrate, the disulfide bond is cleaved forming two Au-S bonds. While the oligo will then be chemisorbed to the gold through this bond, so will the dimethoxytrityl. In order to prevent binding of the dimethoxytrityl to the gold substrate, the oligonucleotide is deprotected before exposure to the gold. This deprotection is a process that breaks the disulfide bond forming a thiol. This is followed by purification in order to remove the demethoxytrityl.

1 ml of 100mM dithiothreitol (DTT, pH 8.4) was added to a dry aliquot (1-10nmol) of oligonucleotides and allowed to react for 30 minutes at room temperature while stirring. Excess DTT and byproducts from the reaction mixture were removed by size exclusion chromatography according to the directions available with the PD-10 columns. 1.0 M potassium phosphate (KP) buffer (pH 7.2) was used for the purification of the probe (R20) and target (T20) oligos. The Sephadex G-25 column, which is stored in 70% ethanol, was conditioned by rinsing with 30ml 30% ethanol, 30ml 10% ethanol, then 30ml of the buffer before adding the oligo. The 1ml reacted oligonucleotide was brought to a volume of 2.5ml using the buffer and added to the column. The oligonucleotide was rinsed through by addition of 30 ml of the buffer; the oligonucleotide was captured in the first 3.5ml. UV-Visible Spectroscopy was used to determined oligo

concentration at λ260nm. The deprotected oligonucleotide solution was stored at -20°C for up to 1 month.

DNA-Gold Bioconjugates. 1ml of 20nM BSPP capped gold colloid was placed in a 4ml vial equipped with a magnetic stirbar. 2.6μL of purified T20 (7.7 μM, 1 equivalent) was diluted with 0.1ml 0.3M NaCl and added dropwise to the colloid solution while stirring vigorously. The solution was brought to a final concentration of 10nM by addition of 0.9 ml of 0.3 M NaCl. The solution was stirred for 1 hour to allow an estimated 1 DNA strand to bind to 1 gold nanoparticle. The solution was used as is for target hybridization or diluted to the appropriate concentration using 1 X SSC hybridization solution. (This solution was stable when scaled up to a 10ml volume of 20nM colloid solution.)

Probe Deposition. The basic scheme for probe deposition and target hybridization is shown if Figure 3.3. A 1 μM solution of 20% R20 oligo (0.2 μM) and 80% Mercaptohexanol (0.8μM, MCH) was prepared in 1.0 M potassium phosphate (KP) buffer (pH 7.4). A fresh solution was made for each preparation due to the decomposition of MCH in solution over time. A 0.5” x 0.5” gold-coated slide was cleaned using piranha (30% hydrogen peroxide (35% in water) and 70% sulfuric acid v/v), rinsed with water, and dried under an argon stream. The gold substrate was then place in the 20% DNA solution for 1 hour for thiol deposition. The gold slide was then removed, rinsed with deionized water, and dried under an argon stream. At this point, the probe monolayer was ready for hybridization. This modified gold slide is used as the working electrode in the electrochemical and photoelectrochemical measurements.

Two alterations were made in the deposition method in order to determine the most efficient way to create the self-assembled monolayer. The goal was to obtain a rapid method with a low background noise. This noise will be discussed in the results. The first alteration was preparing the oligonucleotide/MCH solution in 30% acetonitrile in water rather than 100% water. The second alteration was addition of electrochemical cleaning step of the gold substrate before thiol deposition. The electrochemical cleaning was performed after the piranha cleaning.

For electrochemical cleaning, the gold substrate was placed in the photoelectrochemical cell (Figure 4.4). Electrochemical cleaning was performed using cyclic voltammetry in an aqueous electrolyte solution composed of 0.1 M H_2SO_4 and 0.01 M KCl. The potential was cycled from 0 to 1.7 V vs. Ag/AgCl until a reproducible cyclic voltammogram was observed (Figure 3.6). The electrolyte was then removed and the cell rinsed with water before addition of the 20% R20 / 80% MCH deposition solution. After 1 hour the solution was removed and rinsed with deionized water. The substrate was then ready for hybridization of the target.

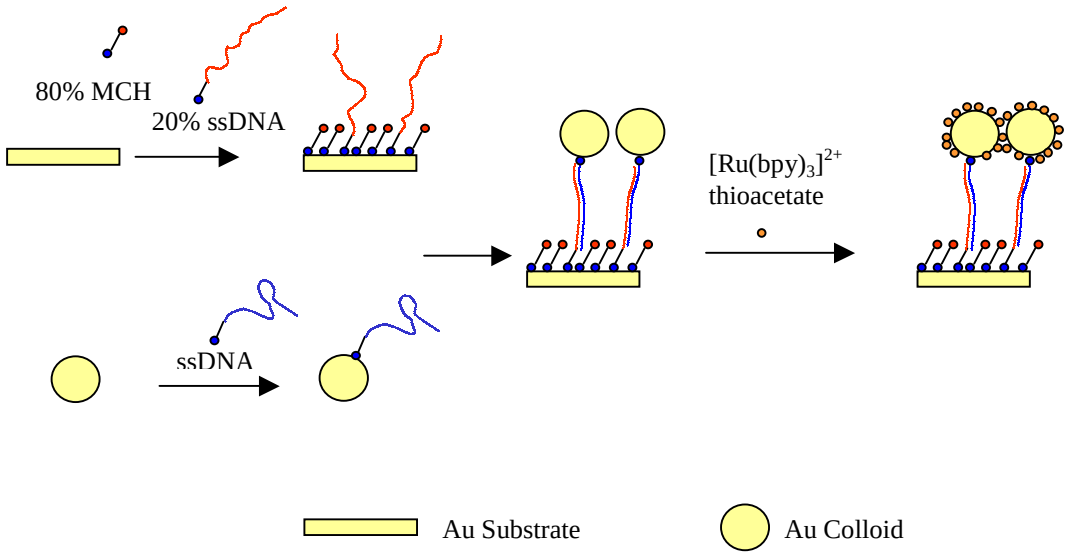

Figure 3.3 SAM Preparation Scheme.

Hybridization and Deposition of Thiolated $[Ru(bpy)_3]^{2+}$. The probe DNA substrates were placed in 20ml vials containing 2ml of DNA-gold bioconjugate, concentrations ranging from 10nM to 0.5nM. The vials were sealed and placed in a water bath at 45ºC. After 1 hour the water bath was turned off allowing the temperature to slowly cool to room temperature over a 16-hour period. The gold substrate was removed from the vial and with deionized water. The substrates were then placed in 1mM aqueous solution of thiolated $[Ru(bpy)_3]^{2+}$ (listed as compound 3 in Chapter 2) for 4 hours to allow the dye-sensitizing molecule to attach to the gold nanoparticles. The substrate was rinsed with deionized water and dried under nitrogen before analysis. The substrate was analyzed using photoelectrochemistry and AFM. The photoelectrochemical results will be discussed in Chapter 4.

3.2.3 Instrumental Setup

Cyclic Voltammetry. Cyclic Voltammetry was used for electrochemical cleaning of the gold slides for SAM modification. An EG&G Princeton Applied Research Potentiostat/Galvanostat Model 273A equipped with EG&G Instruments, Inc. Model 270/250 Research Electrochemistry Software 4.00 was used for all electrochemical measurements. Electrochemical cleaning of the gold working electrodes were accomplished by cycling from 0 to +1.7 V until a reproducible CV was obtained. The cleaning solution was an aqueous electrolyte composed of 0.1 M H_2SO_4 and 0.01 M KCl. A scan rate of 100 mV/s was used with a Ag/AgCl reference electrode and platinum counter.

Optical Absorption Measurements. A Hewlett Packard HP 8453 UV-Visible spectometer was used with HP Chemstation software. The optical density (OD) of oligonucleotides and gold nanoparticles were monitored at 260 nm and 530 nm respectively. A quartz cuvette with a 0.5 cm pathlength was used for all measurements.

Atomic Force Microscopy. Tapping mode AFM was performed using a Digital Instruments Nanoscope IIIa Scanning Probe Microscope with Nanoscope IIIa software Version 4.23r6. This method was used to view the gold substrate to determine the number of gold colloids bound to the substrate through hybridized DNA. An average particle count was obtained per square centimeter.

3.3 Results and Discussion

3.3.1 Target Preparation

The procedures listed above for the preparation of target oligonucleotide attached to gold colloids and probe-MCH mixed monolayer attached to a gold surface have been used over the past few years by various research groups[1,3,4,5]. Attachment of the target to the gold colloid was confirmed in the photoelectrochemical procedure, which will be discussed in the following chapter. According to a study by Alivisatos et al.[6], one equivalent of thiolated DNA added to gold colloid yield anywhere from 0 to 5 DNA strands per particle of gold. This was determined using gel electrophoresis with a 50mer being the shortest oligo separable using this technique. Therefore, this technique could not be employed for our DNA bioconjugates containing oligonucleotides with 20 base pairs.

3.3.2 Probe Deposition

Problems were encountered using the literature preparations for the probe deposition. Figure 3.4 shows a cyclic voltammogram of the 20% R20 oligo 80% MCH monolayer that was prepared in 100% aqueous KP buffer. The anodic current increases as the potential is scanned past 250mV. The cause of this anodic current is unknown, but likely to be some type of oxide that has formed on the gold slide. A peak in this region is also seen during the electrochemical cleaning method.

Electrochemical cleaning was incorporated into the probe preparation in an attempt to remove what appeared to be an oxide on the gold surface. Figure 3.5 shows a cyclic voltammogram of four electrochemical cycles used in the cleaning. The anodic peak at ~1.2V is the oxidative formation of gold oxide and a chloro-aurate complex. The

cathodic peaks at ~0.9V and ~0.7V are the reductive stripping of the gold oxide and the chloro-aurate, respectively. The anodic peak at 0.5V has been previously reported in the

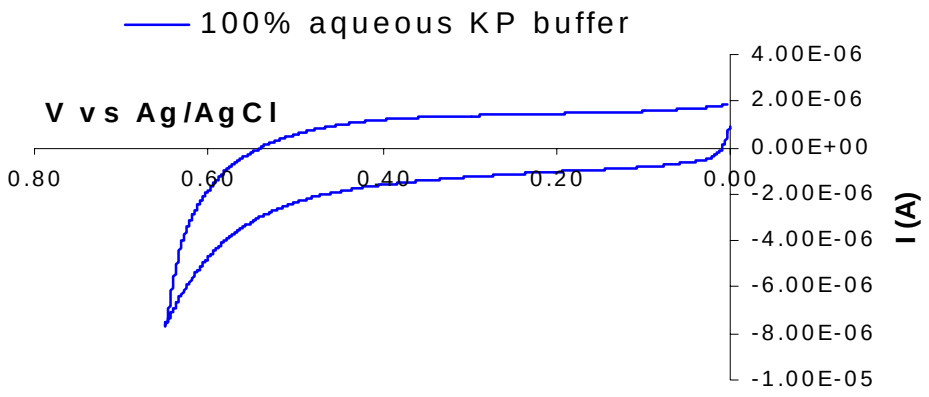

Figure 3.4 Cyclic Voltammogram of 20% Probe / 80% MCH Monolayer. Sample prepared in a 100% aqueous KP buffer (1.0M, pH 7.4). Pt counter electrode. Electrolyte contains 0.1M KP buffer (pH 7.2) and 0.05M EDTA.

literature[7] with much confusion as to this peak is due to. The formation of a low coverage of hydrous oxide was stated as being a possible cause.

Figure 3.6 shows the cyclic voltammogram of the probe/MCH monolayer, deposited from the 100% aqueous probe deposition solution, which underwent electrochemical cleaning before deposition. The anodic faradaic current that appeared in Figure 3.5 is no longer present and the charging current is much reduced. The decrease in charging current may be a result of decreased surface area of the polycrystalline gold surface since electrochemical cleaning is an annealing process. Improvement in the

charging current may also be due to removal of surface oxides on the gold, allowing better coverage of the thiol.

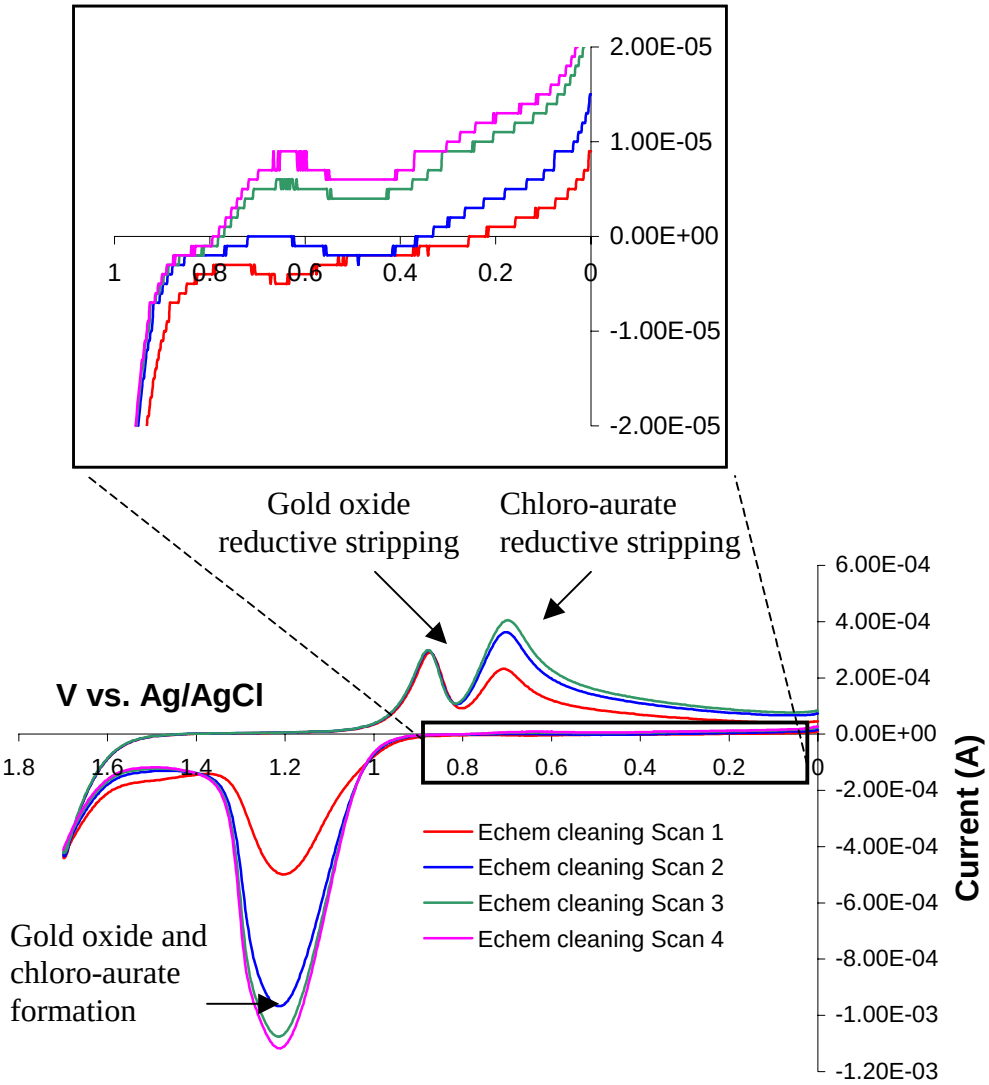

Figure 3.5 Electrochemical Cleaning of Gold Substrate. Pt counter electrode; scan rate 100mV/s; electrolyte consists of 0.01M KCl in 0.1M H_2SO_4. Expanded portion of the anodic current shows a peak of unknown origin.

The second modification of the probe deposition procedure was increasing the solubility of MCH by using a 30% acetonitrile solution for the KP buffer. The electrochemical cleaning was not used in combination with this. The resulting cyclic voltammogram is shown in Figure 3.6. The charging current using this method was identical to that of the electrochemical cleaning method. The use of acetonitrile may facilitate the removal of oxides on the gold surface allowing better coverage of the oligonucleotide probe and MCH on the gold surface.

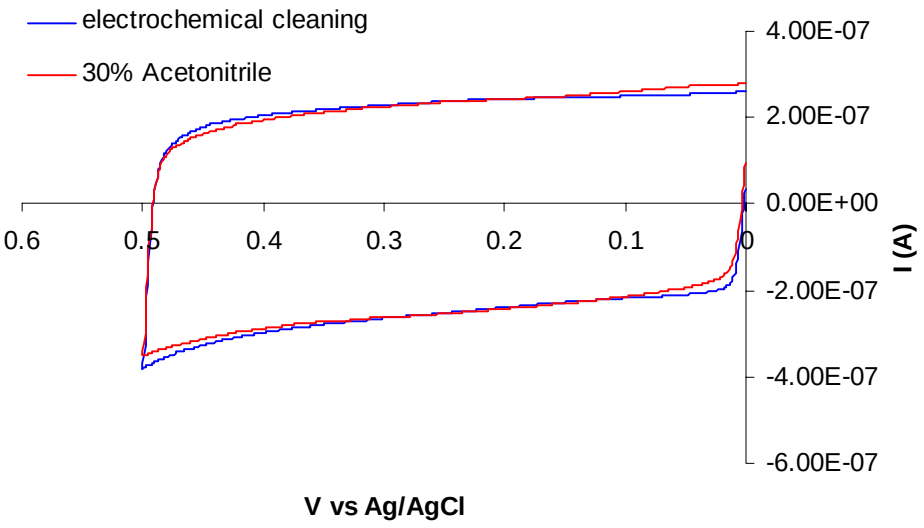

Figure 3.6 Cyclic Voltammogram of 20% Probe / 80% MCH Monolayer after Procedure Modifications. Pt counter electrode. Electrolyte contains 0.1M KP buffer (pH 7.2) and 0.05M EDTA.

3.3.3 Atomic Force Microscopy

The target oligonucleotide is covalently attached to a gold colloid as described previously. When the target hybridizes with its complementary probe strand on the polycrystalline gold substrate, tapping mode atomic force microscopy (AFM) can be employed to visually see the colloids. As the microscope tip taps across the gold substrate an apparent height image is obtained. The 10nm gold colloids are higher than the gold surface, so they appear as yellow dots on the AFM images. Figure 3.7 demonstrates an increase in target hybridization with an increase in target concentration. Figure 3.8, a plot of particles/cm^2 vs. target concentration, demonstrates that hybridization is directly proportional to target concentration.

A probe slide was also exposed to a 6nM solution of a non-complementary target. The AFM image is shown in Figure 3.9 and also plotted in Figure 3.8. The results showed a small amount of non-specific binding which is in agreement with previous studies[8,9].

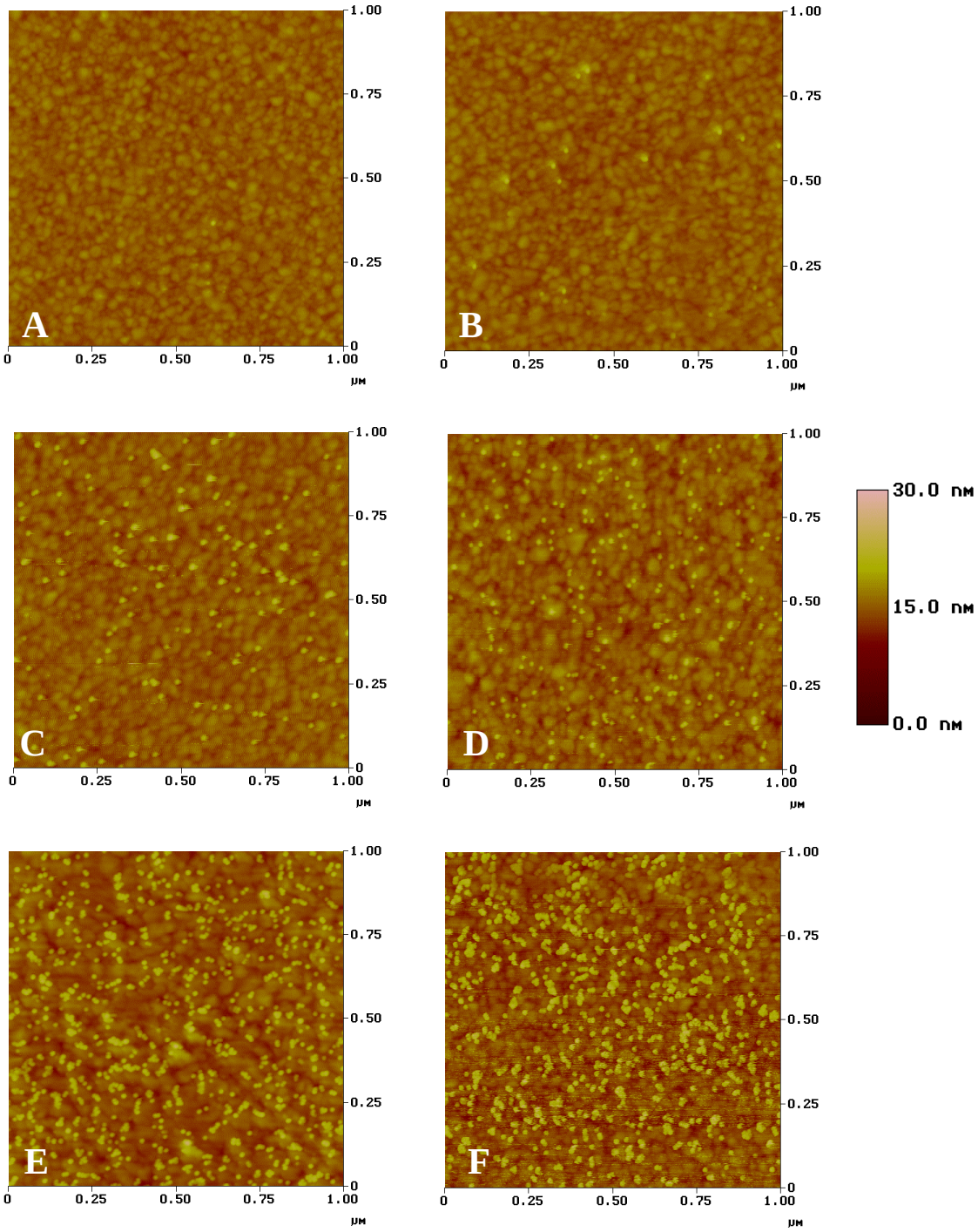

Figure 3.7 AFM Images of Gold Substrate after Target Hybridization. Target solution at various concentrations during hybridization: 0.25nM (A), 0.50nM (B), 1.0nM (C), 2.0nM (D), 4.0nM (E), and 6.0nM (F).

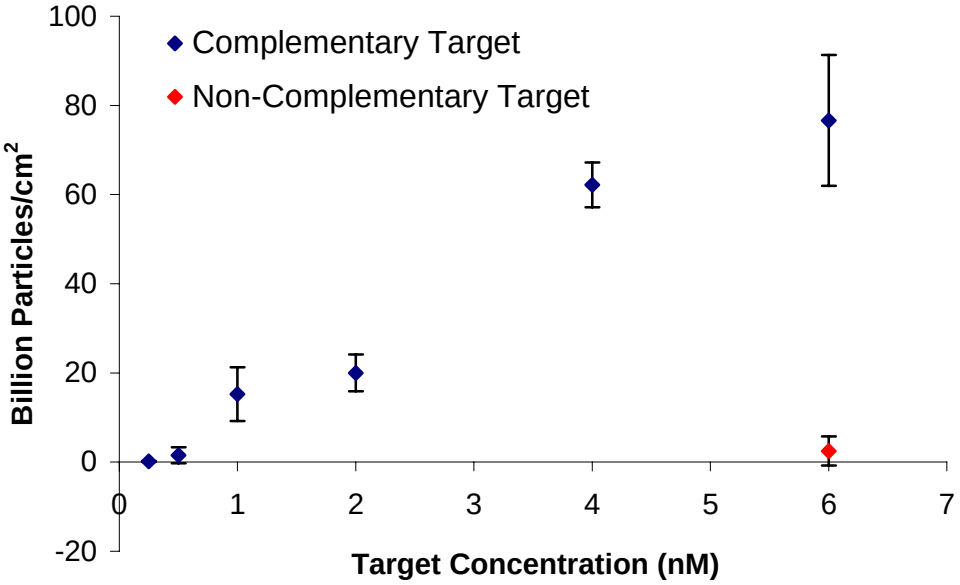

Figure 3.8 Target Concentration vs. # of Particles.

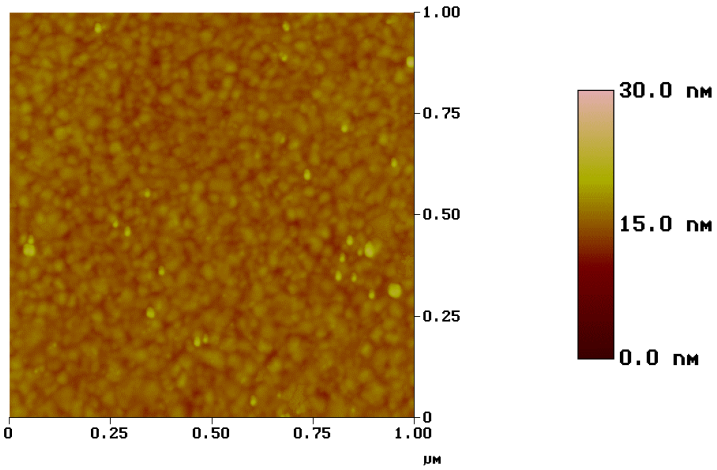

Figure 3.9 AFM Images of Gold Substrate after Non-Complementary Target Hybridization. Target solution at 6.0nM.

3.4 References

[1] Sauthier, M.L., Carroll, R.L., Gorman, C.B., and Franzen, S. Nanoparticle layers assembled through DNA hybridization: characterization and optimization. *Langmuir* **2002**, 18, 1825-1830.

[2] Loweth, C.J., Caldwell, W.B., Peng, X., Alivisatos, A.P., and Schultz, P.G. DNA-based assembly of gold nanocrystals. *Angew. Chem. Int. Ed.* **1999**, 38, No. 12, 1808-1812.

[3] Taton, T.A., Mucic, R.C., Mirkin, C.A., and Letsinger, R.L. The DNA-mediated formation of supramolecular mono- and multilayered nanoparticle structures. *J. Am. Chem. Soc.* **2000**, 122, 6305-6306.

[4] Herne, T.M., and Tarlov, M.J. Characterization of DNA probes immobilized on gold surfaces. *J. Am. Chem. Soc.* **1997**, 119, 8916-8920.

[5] Storhoff, J.J., Elghanian, R., Mucic, R.C., Mirkin, C.A., and Letsinger, R.L. One-pot colorimetric differentiation of polynucleotides with single base imperfection using gold nanoparticle probes. *J. Am. Chem. Soc.* **1998**, 120, 1959-1964.

[6] Zanchet, D., Micheel, C.M., Parak, W.J., Gerion, D., and Alivistatos, A.P. Electrophoretic isolation of discrete Au nanocrystal/DNA conjugates. *Nanoletters* **2001**, 1, 32-35.

[7] Zu, Y. and Bard, A.J. Electrogenerated chemiluminescence. 66. The role of direct coreactant oxidation in the ruthenium tris (2,2') bipyridyl/tripropylamine system and the effect of halide ions on the emission intensity. *Anal. Chem.* **2000**, 72, 3223-3232.

[8] Thiel, A.J., Frutos, A.G., Jordan, C.E., Corn, R.M., and Smith, L.M. In situ surface plasmon resonance imaging detection of DNA hybridization to oligonucleotide arrays on gold surfaces. *Anal. Chem.* **1997**, 69, 4948-4956.

[9] He, L., Musich, M.D., Nicewarner, S.R., Salinas, F.G., Benkovic, S.J., Natan, M.J., and Keating, C.D. Colloidal Au-enhanced surface plasmon resonance for ultrasensitive detection of DNA hybridization. *J. Am. Chem. Soc.* **2000**, 122, 9071-9077.

Chapter 4: Photoelectrochemical Detection of DNA Hybridization

4.1 Introduction

Photoelectrochemistry of $[Ru(bpy)_3]^{2+}$ attached to a gold substrate has only recently been studied. In 1997 a study by Yamada et. al.[1] first demonstrated photocurrent from $[Ru(bpy)_3]^{2+}$ attached to a gold substrate via a thiol. The molecule studied in this research is shown in Figure 4.1. Yamada's molecule is similar to the molecule used in this thesis research with one difference being the number of carbons within the alkane chain. The $[Ru(bpy)_3]^{2+}$ molecule in this thesis contains a 6-carbon alkane chain while the molecule reported by Yamada contained 17 carbons. A later study by Koide et al.[2] focused on the effects of the spacer-chain length between this photoredox-active molecule and thiol. The results showed that the molecule with 17 carbons demonstrated a very low current due to photoexcitation. This photocurrent was even lower using the molecule containing a 13-carbon alkane chain. The reason for a decrease in photocurrent was unclear, however, a possibility could be the rate of electron transfer over varying distance along the alkane chain competing with other rates as shown in Figure 4.2. According to the results of these previous studied a photocurrent may not be observed when the molecule of interest in this thesis is directly attached to a gold surface.

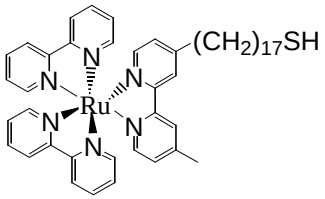

Figure 4.1 Molecule Studied by Yamada et.al.

The self-assembled monolayer studied in this thesis does not focus on the attachment of the thiolated $[Ru(bpy)_3]^{2+}$ molecule directly to the gold substrate. The molecule is separated from the gold substrate by a dsDNA molecule as well as a 10nm diameter gold nanoparticles as demonstrated in Figure 4.3. Electron transfer through

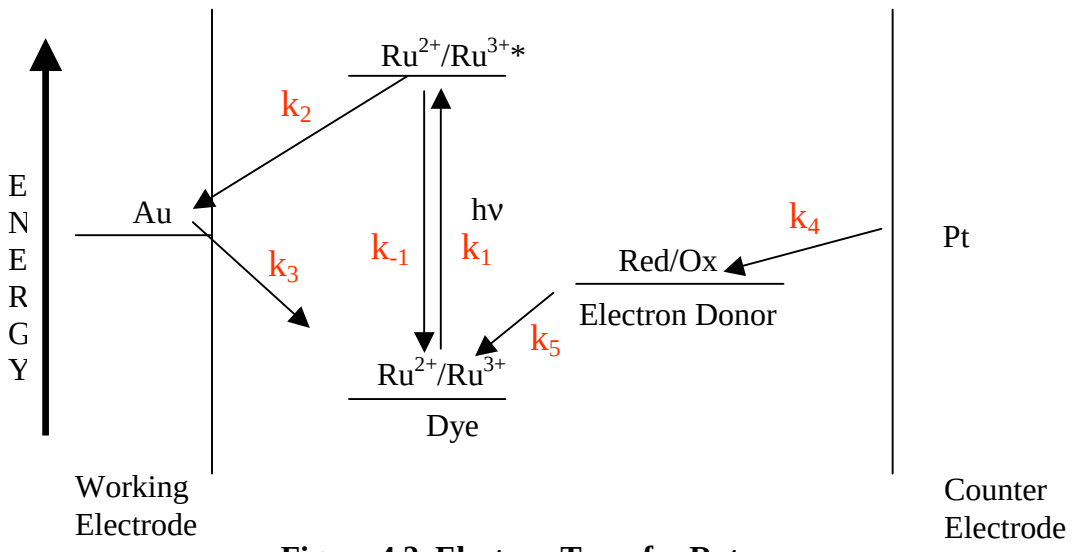

Figure 4.2 Electron Transfer Rates

DNA has already been discussed in Chapter 1 and appears to be a suitable mode of transport for the electrons in this photoelectrochemical system. Electron transfer from ruthenium complexes to a working electrode through gold nanoparticles has also been demonstrated in previous work[3,4].

The prior knowledge obtain about surface-attached $[Ru(bpy)_3]^{2+}$ supports the idea that the photoelectrochemical system designed in this thesis for DNA hybridization detection is a feasible method. While the basic design is a series of Au-S bonds that have been well studied, other details of the setup must be carefully considered, especially the sacrificial electron donor within the photoelectrochemical system and its concentration as well as the voltage range which is non-destructive for the working electrode (modified Au substrate).

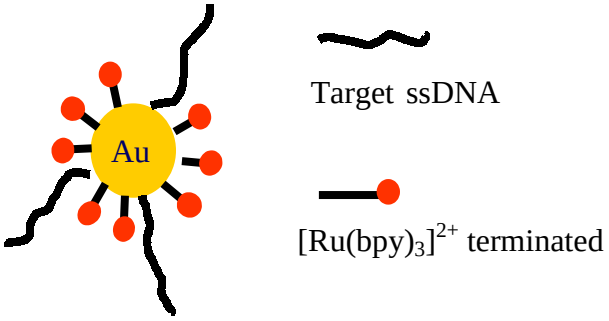

Figure 4.3 Target Oligo with $[Ru(bpy)_3]^{2+}$ Marker

4.2 Experimental

4.2.1 Materials

All chemicals were used as received from vendors without further purification. Triethanolamine, tripropylamine, and triethylamine were supplied by Aldrich. Fisher Scientific supplied disodium ethylenediaminetetraacetic acid (EDTA). Mallinckrodt supplied potassium phosphate monobasic.

4.2.2 Instrumental Setup

Cyclic Voltammetry. An EG&G Princeton Applied Research Potentiostat/Galvanostat Model 273A equipped with EG&G Instruments, Inc. Model 270/250 Research Electrochemistry Software 4.00 was used for all electrochemical measurements. Cyclic Voltammetry was used for the characterization of the electron donor using a 0.071cm^2 gold working electrode, a Pt counter electrode, and a Ag/AgCl reference electrode at a scan rate of 100 mV/s. The electrolyte was 0.1M aqueous potassium phosphate (pH 7.2). The sample was purged for 15 minutes with nitrogen before analysis. The potential was scanned from 0 to 1V vs Ag/AgCl. The reductants tested are listed in Figure 4.5. The oxidative stripping potential of thiol on a gold surface was also investigated to determine a non-destructive potential range for photoelectrochemical measurements. The potential was cycled multiple times from 0 to 1.7V vs. Ag/AgCl with a Pt counter electrode.

Photoelectrochemistry. The light source for the photoelectrochemical measurement was a Oriel Instruments 75 W Xenon arc lamp operated using an Oriel 68806 Basic Power Supply (50-200 W). The Photoelectrochemical cell was connected to

an EG&G Princeton Applied Research Potentiostat/Galvanostat Model 273A equipped with EG&G Instruments, Inc. Model 270/250 Research Electrochemistry Software 4.00. The diagram for the experimental setup is in Figure 4.4. The optical window and working electrode each have an area 0.38 cm^2. The working electrode was irradiated with a light intensity of 0.64 W/cm^2. The electrolyte was composed of 0.1 M KP buffer (pH 7.2).

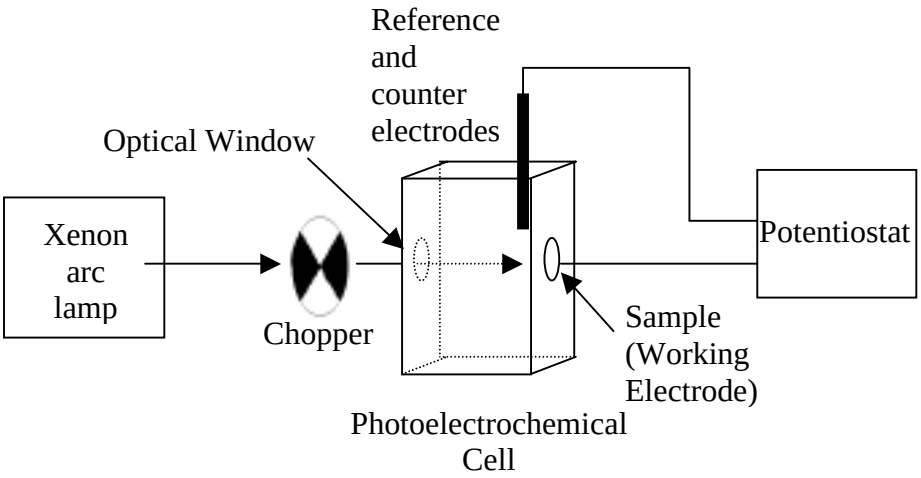

Figure 4.4 Photoelectrochemical Setup.

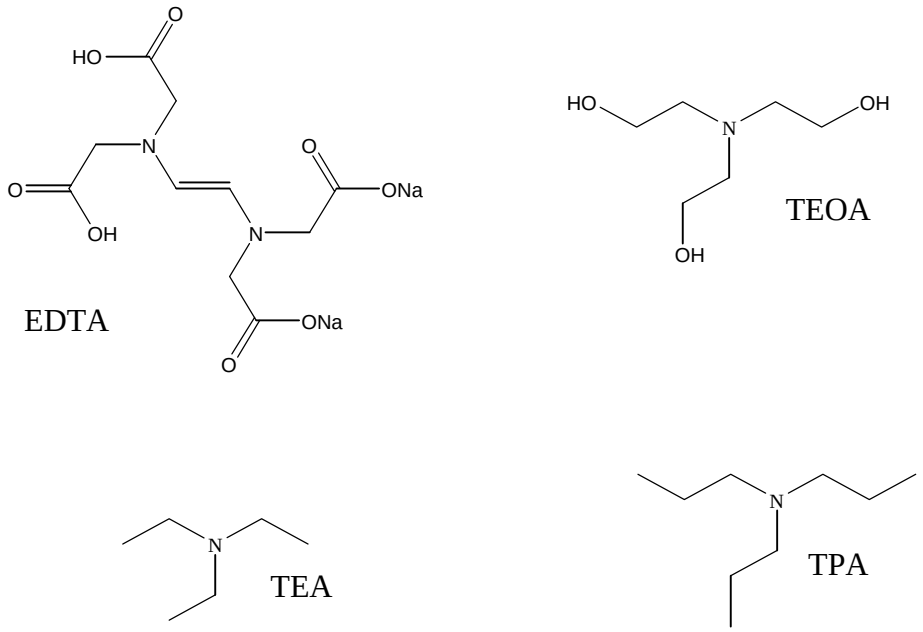

Figure 4.5 Common Molecules Used as an Electron Donor for $[Ru(bpy)_3]^{2+}$ in Photoelectrochemical Experiments.
Ethylenediaminetetraacetic Acid, Disodium Salt (Na_2EDTA), Triethanolamine (TEOA), Triethylamine (TEA), and Tripropylamine (TPA).

4.3 Results and Discussion

This section is separated into three parts. The first section focuses on the backgound photoelectrochemical (PEC) signal which is effected by the sacrificial electron donor. It also discusses the potential range in which the PEC experiments can be performed without destruction of the modified gold substrate. The second section concentrates on the control experiments. The this section investigates the effect of applied potential as well as target concentration on the PEC response.

4.3.1 Photoelectrochemical Light and Dark Background Currents.

Many factors must be considered when designing a dye-sensitized photoelectrochemical (PEC) system, such as the dye, the sacrificial electron donor, and the potential at which the experiments will be performed. The dye used in the following experiments was $[Ru(bpy)_3]^{2+}$. This section discusses the selection of an electron donor as well as focuses on the potential window in which the PEC experiments may be performed. Both parameter are important for optimizing the experimental conditions.

In the photoelectrochemical experiments the working electrode, which is the DNA-modified gold substrate, was held at a constant potential and the current monitored. The dark current (Figure 4.6) is defined as the current when the sample is not being illuminated by the Xe arc lamp. Upon illumination, the anodic current increases due to photoexcitation. The photocurrent (I_{PC}) is defined in equation 4.1.

$$I_{PC} = \left| I_{light\ on} - I_{light\ off} \right| \qquad 4.1$$

The sacrifical electron donor of the PEC system was investigated in order to obtain a low dark current. Due to their common use in chemiluminescent and PEC systems for $[Ru(bpy)_3]^{2+}$, disodium ethylenediaminetetraacetic acid (EDTA), triethanolamine (TEOA), triethylamine (TEA), and tripropylamine (TPA) were tested. If the oxidation potential of the electron donor is less than the potential used in the PEC experiments, the electron donor at the electrode surface will undergo an oxidation causing an increased anodic current. Due to the high concentration of donor (50mM), it may take hours for the dark current to decrease while at a constant potential.

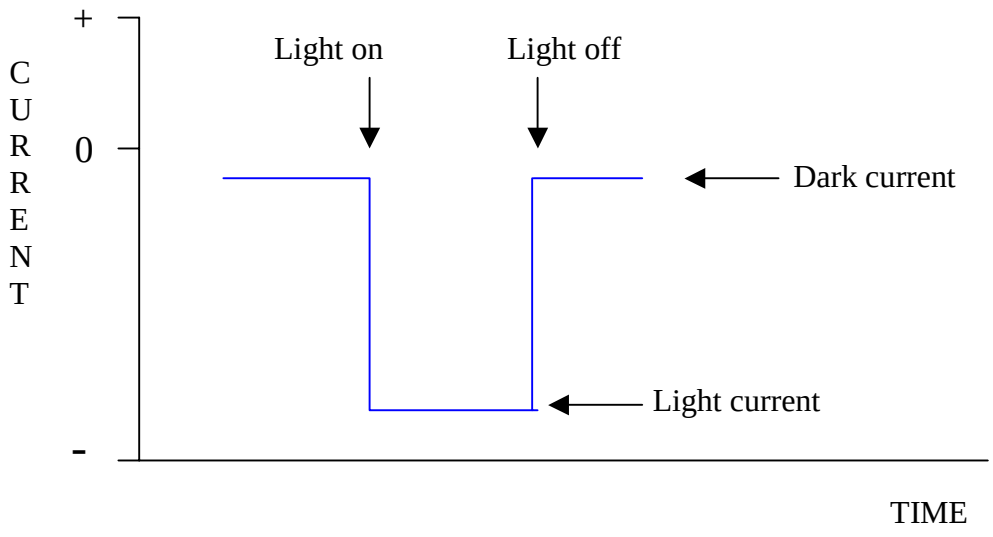

Figure 4.6 Photocurrent Response.

Cyclic voltammetry was used to monitor the reduction potential of these four compounds. The cyclic voltammograms are shown if Figure 4.7. Tertiary amines undergo two oxidations as shown in equations 4.2 and 4.3, using TPA as an example, with the second oxidation being irreversible.

$$Pr_3N - e^- \longrightarrow Pr_3N^{\bullet +} \longrightarrow Pr_2\overset{\bullet}{N}CHEt + H \qquad 4.2$$

$$Pr_2\overset{\bullet}{N}CHEt - e^- \longrightarrow Pr_2N^+{=}CHEt \qquad 4.3$$

The expanded view in Figure 4.7 shows the first oxidation of TPA starting at a potential lower that 0V, TEA at approximately 0V, and TEOA around 0.25V vs. Ag/AgCl. These three molecules would yield a high dark current when working in a potential range of 0.25V to 0.65V. EDTA oxidation starts at 0.75V, which allows it to retain a low dark current up to this, potential. Figure 4.8 demonstrates this improvement in dark current by comparing TEOA and EDTA. The potential was held at 0.5V vs. Ag/AgCl with the modified electrode of dsDNA – 10nm Au colloid – $[Ru(bpy)_3]^{2+}$. The dark current of the TEOA is ~750nA after 25 seconds while that of EDTA falls to less than 100nA within the first second. EDTA was used as the sacrificial electron donor in the following experiments.

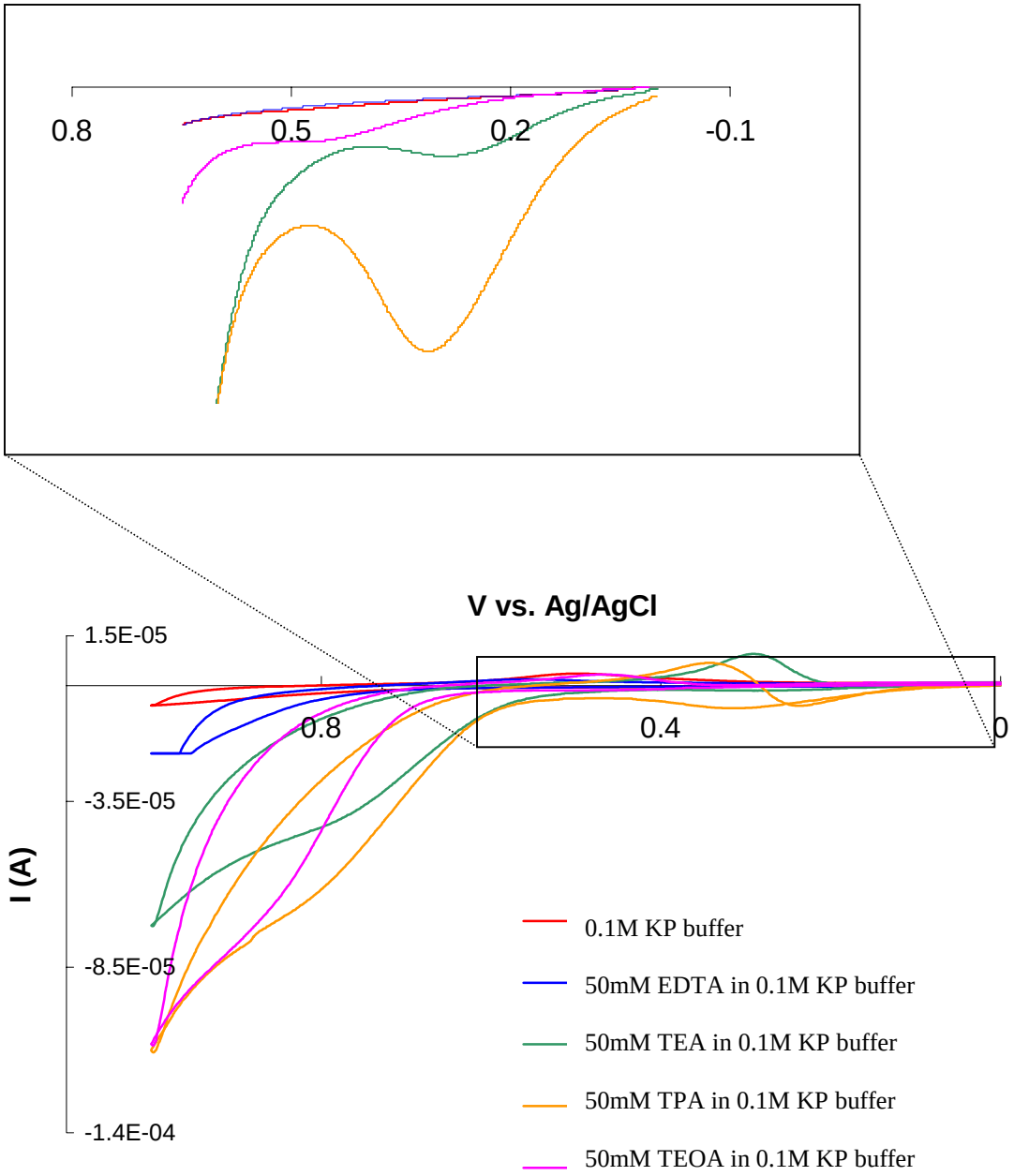

Figure 4.7 Cyclic Voltammogram of Electron Donors.

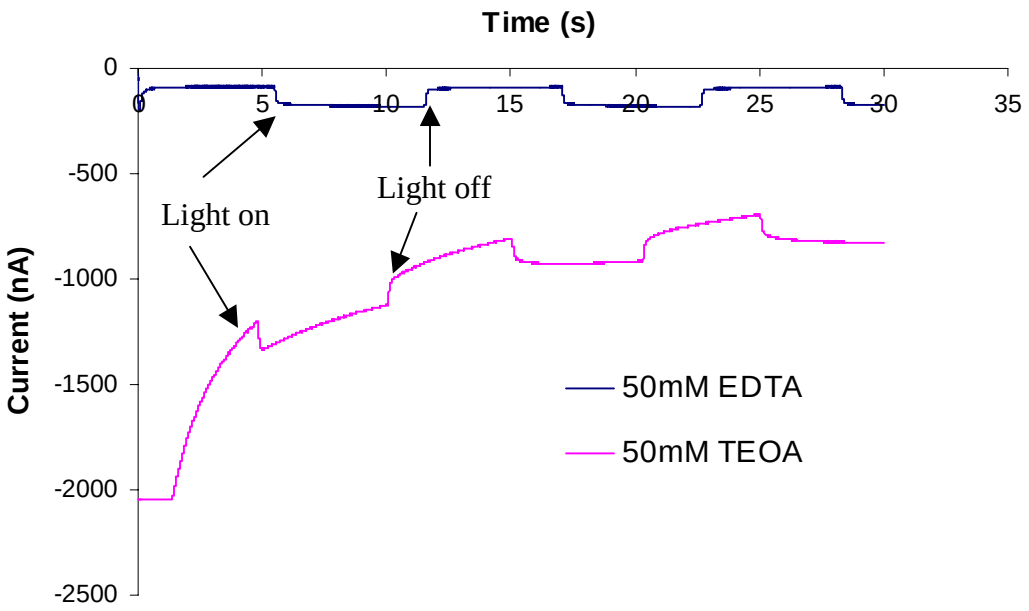

Figure 4.8 Dark Current: TEOA vs. EDTA.

Using EDTA as an electron donor allows a working potential range of 0 to 0.75V vs. Ag/AgCl, however, at high potentials the thiol monolayer is destroyed due to oxidative desorption from the gold substrate. The equation for thiol desorption is in equation 4.4.

$$RCH_2S - Au + 14\ OH^- \longrightarrow SO_4^{2-} + RCO_2^- + 8\ H_2O + 11\ e + Au \qquad 4.4$$

A 20% probe monolayer was tested in order to determine the potential at which thiol desorbs. This desorption has previously been reported at a potential just above 0.75V vs. SCE in a 0.15M phosphate buffer (pH 7.5)[5]. Figure 4.9 shows the thiol stripping results from the 20% probe monolayer in 0.1M KP buffer (pH 7.2). The potential was cycled 3 times. The first cycle shows oxidative thiol desorption starting at 0.8V vs. Ag/AgCl,

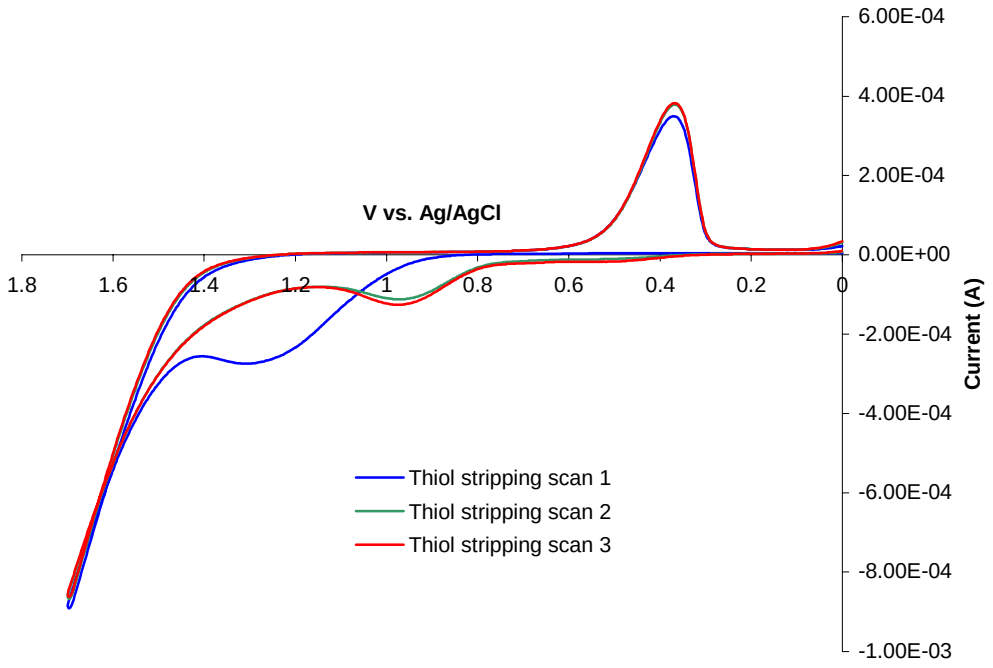

Figure 4.9 Thiol Desorption. 0.1M KP buffer, Pt counter electrode, working electrode modified with 20% probe and 80% MCH.

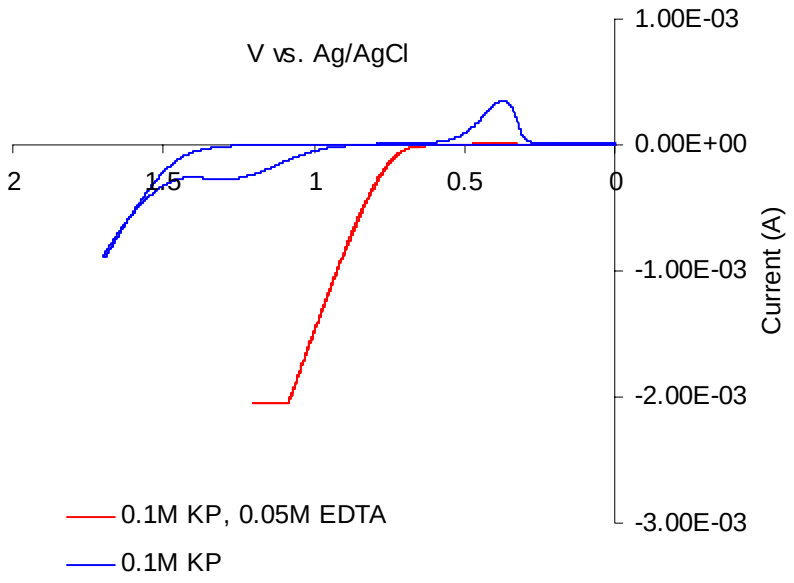

Figure 4.10 Thiol Desorption in the Presence of EDTA. Pt counter electrode, working electrode modified with 20% probe and 80% MCH.

which is in close agreement with previous results. The cathodic peak observed is the reductive gold oxide stripping. (This is not comparable to the gold oxide stripping seen in Figure 3.6 due to varying electrolytes.) The second and third scans resulted in anodic formation and reductive stripping of gold oxide. Thiol desorption was also attempted in the 0.1M KP buffer with 0.05M EDTA (Figure 4.10). The thiol desorption peak was not visible above the oxidative current of EDTA and only a small gold oxide reduction peak was visible in the cathodic current. According to the lack of gold oxide stripping it appeared that the thiol layer was not being destroyed even after numerous cycles. For this monolayer the electrolyte solution was switched back to 0.1M KP buffer without EDTA, and thiol desorption was observed. Due to the high concentration of EDTA a competition for electrons may have been present with more electrons being donated to EDTA rather than the oxidation process of thiol desorption.

4.3.2 Control Experiments.

As mentioned in Chapter 3 after hybridization the modified gold substrate was placed in a 1mM aqueous solution on the thiolated $[Ru(bpy)_3]^{2+}$ for four hours for the molecule to chemisorb to the Au colloids. This molecule contains a thioacetate, as shown if Figure 2.3, rather than a thiol. While a thiol will adsorb to a gold substrate within seconds, it often takes hours for the thioacetate to form a Au-S bond due to the acetyl-protecting group. This long deposition time was of concern due to the possibility of the thiol displacement on the surface of the gold, i.e., the thiolated $[Ru(bpy)_3]^{2+}$

displacing the MCH or DNA. Control experiments were performed in order to investigate this issue.

In order to determine if displacement was occurring a 100% MCH monolayer was exposed to the $[Ru(bpy)_3]^{2+}$ molecule for four hours. The PEC data is shown in Figure 4.11. TEOA was used as the electron donor in this PEC system, which is the cause of the dark current variation. The results showed unexpectedly that a MCH monolayer produces a photocurrent of about 50nA. A very slight decrease in photocurrent was observed after the modified Au substrate was exposed to the $[Ru(bpy)_3]^{2+}$ molecule.

A second control was used to help confirm that the monolayer thiol was not being displaced. In the target preparation, a non-thiolated target oligo was mixed with the Au colloid. Since the oligo did not contain a thiol it should not bond with the colloid resulting in free oligo in solution with Au colloid. A probe substrate was hybridized in this solution and then exposed to the thiolated $[Ru(bpy)_3]^{2+}$. The target was expected to hybridize resulting in dsDNA, however, the Au colloid should stay in solution and rinsed away before $[Ru(bpy)_3]^{2+}$ deposition. The PEC results in Figure 4.12 show virtually no change in photocurrent for the dsDNA after exposure to the thiolated $[Ru(bpy)_3]^{2+}$. Again, the variation in dark current is due to the use of TEOA as the electron donor in the PEC system.

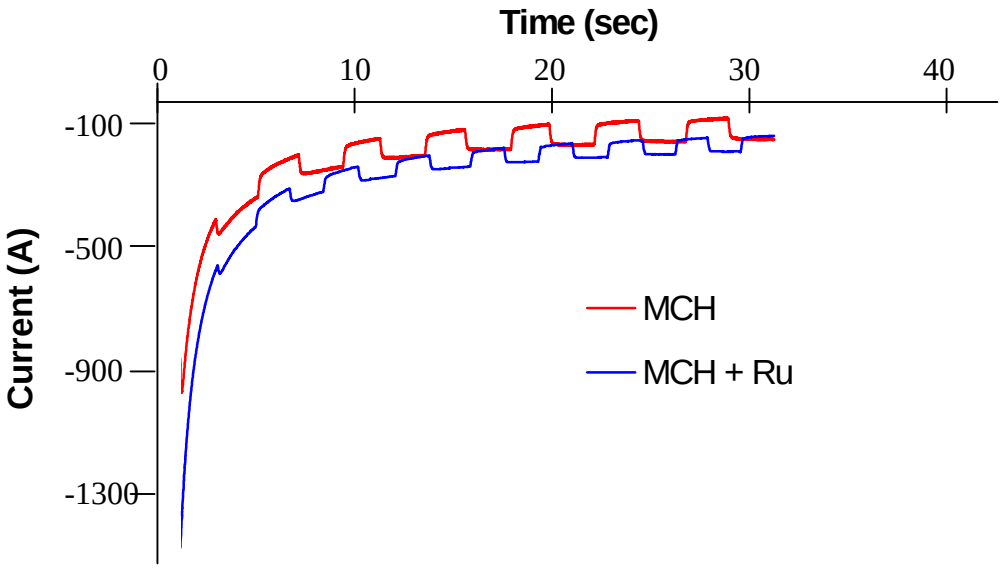

Figure 4.11 $[Ru(bpy)_3]^{2+}$ Deposition Control 1. Modified gold working electrode; Ag/AgCl reference electrode; Pt counter electrode; electrolyte 0.1M KP buffer (pH 7.2) and 0.05M TEOA.

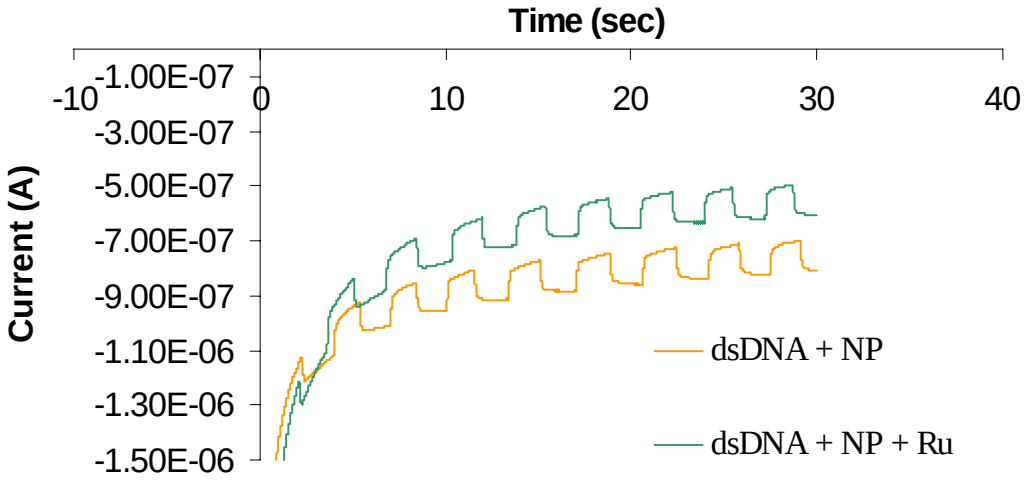

Figure 4.12 $[Ru(bpy)_3]^{2+}$ Deposition Control 2. Modified gold working electrode; Ag/AgCl reference electrode; Pt counter electrode; electrolyte 0.1M KP buffer (pH 7.2) and 0.05M TEOA.

Figure 4.13 demonstrates that the 20% probe / 80% MCH monolayer produces a photocurrent of approximately 40nA. This photocurrent appears to be a result of MCH since the bare gold electrode does not produce a photocurrent and the photocurrent was present with a 100% MCH monolayer. A study by Qingwen et.al.[6] indicates that a portion of the photocurrent may also be due to the oligonucleotide. A slight increase in photocurrent was noted after the probe was hybridized in a 1nM target solution (target attached to Au colloid via Au-S bond) before the thiolated $[Ru(bpy)_3]^{2+}$ was added. A large increase in photocurrent is observed after the thiolated $[Ru(bpy)_3]^{2+}$ is attached to the gold nanoparticle.

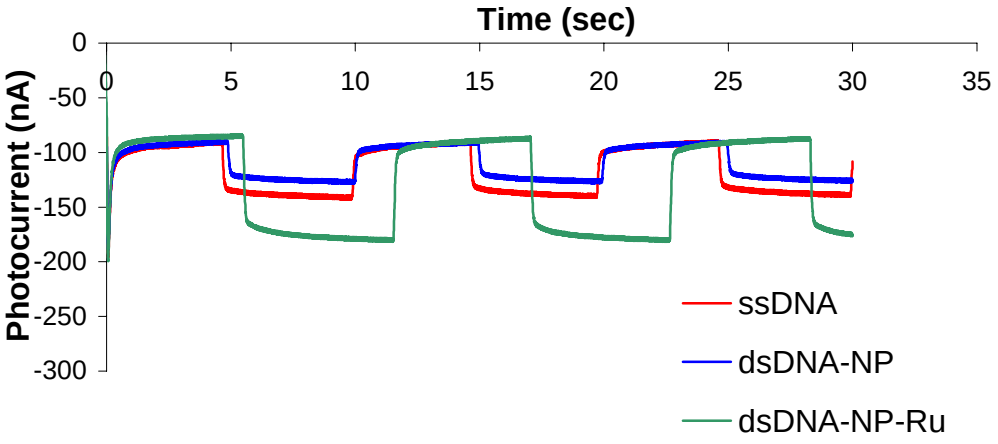

Figure 4.13 PEC Comparison of Probe Before and After Hybridization. Modified gold working electrode; hybridized in a 1nM target solution; Pt counter electrode; electrolyte 0.1M KP, 0.05M EDTA.

4.3.3 Oligonucleotide Detection.

This section presents the photoelectrochemical detection of DNA hybridization using the dye-sensitizing molecule $[Ru(bpy)_3]^{2+}$. The PEC response from this system is effected by the applied potential as well as the concentration of $[Ru(bpy)_3]^{2+}$. The concentration of the dye is directly related to the amount of target that hybridizes. These two issues are discussed in the section.

A 20% probe oligo on gold substrate was prepared as stated in Chapter 3 and hybridized to the target oligo – Au colloid that was at a concentration of 10nM. This sample was used to monitor the effect of applied potential on photocurrent. The photocurrent results are shown if Figure 4.14. The potential was held in a range from 0.1V to 0.5V vs. Ag/AgCl with the light chopped at 0.5Hz. I_{PC} was plotted against potential in Figure 4.15. An exponential increase in photocurrent was observed with increasing potential up to 0.5V. Figure 4.16 demonstrates linear sweep voltammetry from 0 to 0.55V vs. Ag/AgCl as another method to observe the dependence of potential on photocurrent.

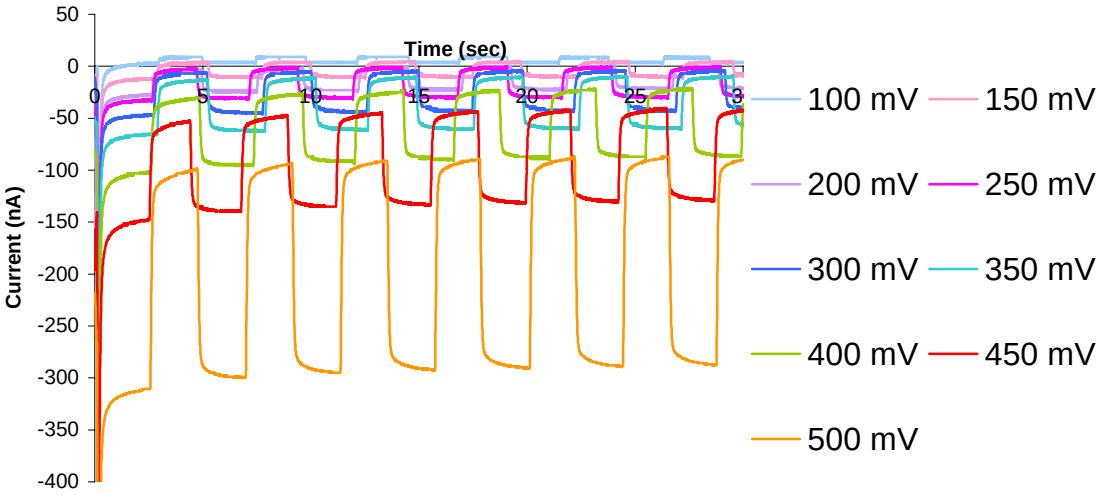

Figure 4.14 Potential Dependence of Photocurrent. Working electrode modified with 20% probe / 80% MCH and hybridized in a 10nM target solution; Pt counter electrode; electrolyte 0.1M KP, 0.05M EDTA.

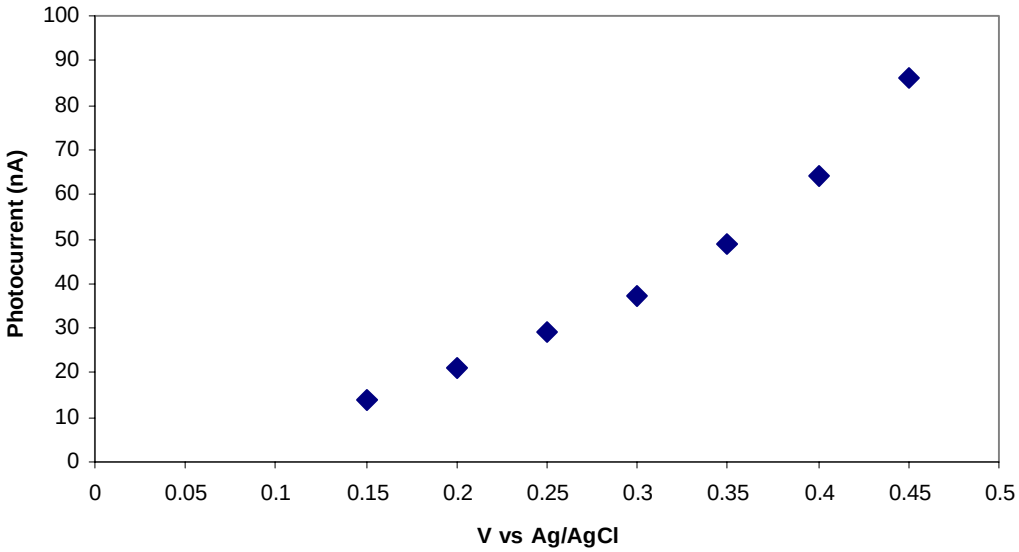

Figure 4.15 Photocurrent vs. Potential. Working electrode modified with 20% probe / 80% MCH and hybridized in a 10nM target solution; Pt counter electrode; electrolyte 0.1M KP, 0.05M EDTA.

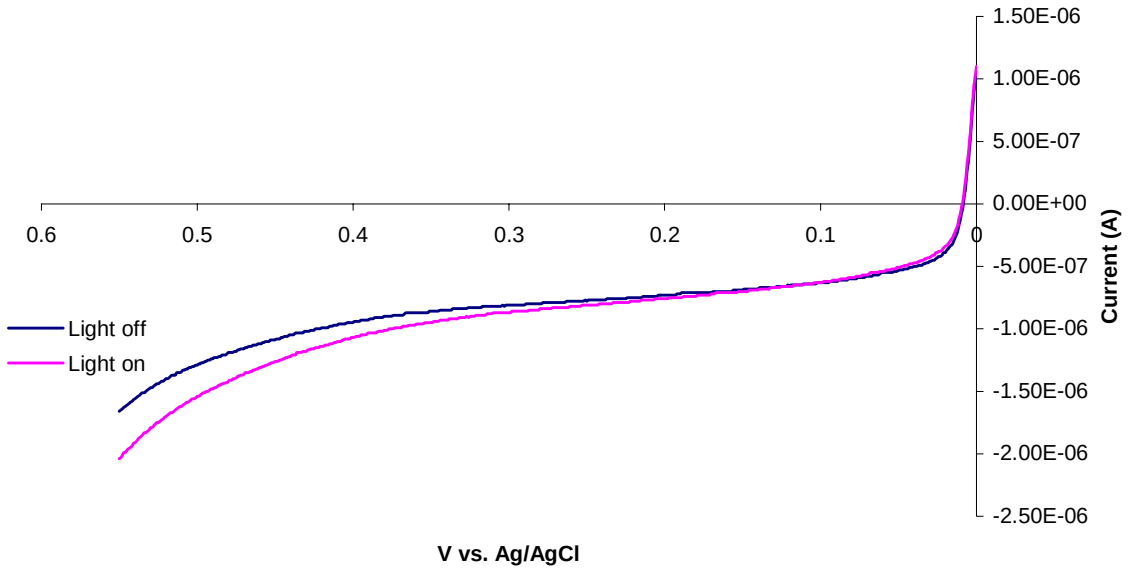

Figure 4.16 Dependence of Potential on Photocurrent using Linear Sweep Voltammetry. Working electrode modified with 20% probe / 80% MCH and hybridized in a 10nM target solution; Pt counter electrode; electrolyte 0.1M KP, 0.05M EDTA.

A calibration curve was created by hybridizing a probe substrate in target solutions concentrations varying from 0.5nM to 10nM. The PEC results are displayed in Figure 4.17 with I_{PC} plotted against concentration in Figure 4.18. The data point at a concentration of 5nM exhibited a much lower I_{PC} than was expected. This low value may be due to an error in sample preparation. Additional calibration curves need to be acquired in order to obtain a more accurate calibration curve.

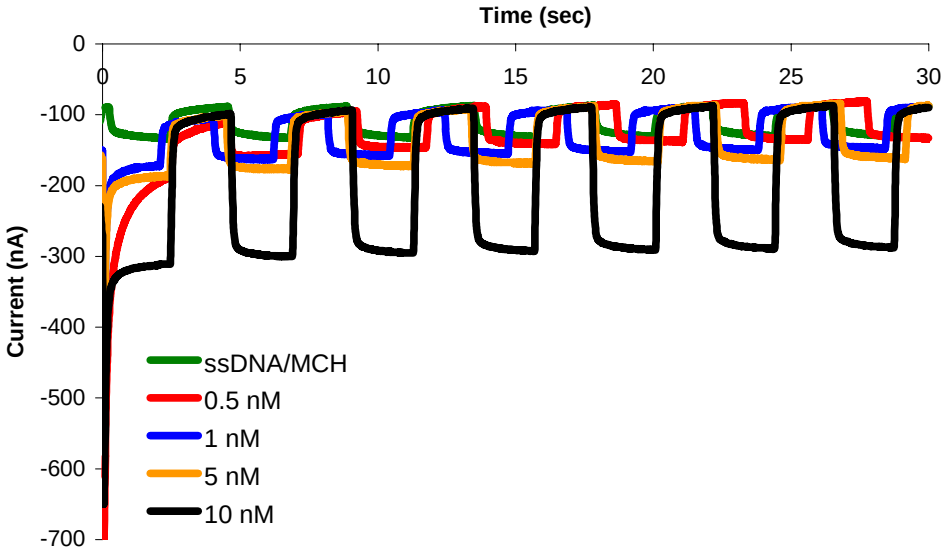

Figure 4.17 PEC Results for Calibration Curve. Working electrode modified with 20% probe / 80% MCH and hybridized in varying concentrations of target solution; Pt counter electrode; electrolyte 0.1M KP, 0.05M EDTA.

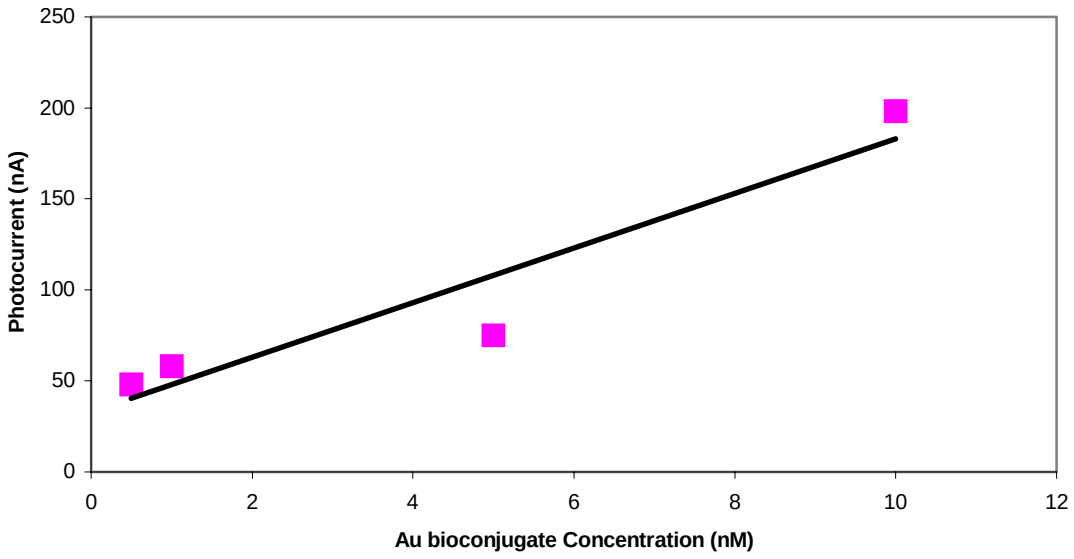

Figure 4.18 Calibration Curve. Working electrode modified with 20% probe / 80% MCH and hybridized in varying concentrations of target solution; Pt counter electrode; electrolyte 0.1M KP, 0.05M EDTA.

4.3 References

[1] Yamada, S., Koide, Y., and Matsuo, Y. A photoresponsive molecular assembly consisting of ruthenium (II) tris(2,2'-bipyridine) – viologen linked disulfide and hexadecanethiol prepared on a gold surface: effect of viologen moiety. *J. Electroanal. Chem.* **1997**, 426, 23-26.

[2] Koide, Y., Terasaki, N., Akiyama, Y., and Yamada, S. Effects of spacer-chain length on the photoelectrochemical responses of monolayer assemblies with ruthenium tris(2,2'-bipyridine) – viologen linked disulfides. *Thin Solid Films* **1999**, 350, 223-227.

[3] Kuwahara, Y., Akiyama, T., and Yamada, S. Facile fabrication of photoelectrochemical assemblies consisting of gold nanoparticles and a tris(2,2'-bipyridine) ruthenium (II) – viologen linked thiol. *Langmuir* **2001**, 17, 5714-5716.

[4] Lahav, L., Geleg-Shabtai, V., Wasserman, J., Katz, E., Willner, I., Dürr, H., Hu, Y.-Z., and Bossmann, S.H. Photoelectrochemistry with integrated photosensitizer – electron acceptor and Au-nanoparticle arrays. *J. Am. Chem. Soc.* **2000**, 122, 11480-11487.

[5] Zu, Y. and Bard, A.J. Electrogenerated chemiluminescence. 67. Dependence of light emission of the tris(2,2')bipyridylruthenium (II) / tripropylamine system on electrode surface hydrophobicity. *Anal. Chem.* **2001**, 73, 3960-3964.

[6] Qingwen, L., Guoan, L., Jun, F., Dawen, C., and Qi, O. Photoelectrochemistry as a novel strategy for DNA hybridization detecton. *Analyst* (Cambridge, United Kingdom) **2000**, 125, 1908-1910.